Palaeontologia Electronica
palaeo-electronica.org

Skeletal atlas of the Thylacine *(Thylacinus cynocephalus)*

Natalie M. Warburton, Kenny J. Travouillon, and Aaron B. Camens

ABSTRACT

The extinct Thylacine *Thylacinus cynocephalus,* also known as the marsupial wolf or Tasmanian Tiger, is an iconic part of Australia's natural history. The latest surviving member of the diverse family Thylacinidae, the thylacine was widespread across mainland Australia during the Pleistocene but by 3200 ybp it was restricted to Tasmania. Persecuted by farmers, thylacines are thought to have gone extinct in the wild by the 1930s, and the last surviving captive animal died in 1936. Despite much public interest and numerous popular accounts, the ecology of this iconic Australian species is not well known. Though huge numbers of animals were killed during the extermination of thylacines from Tasmania, very few useful specimens exist in collections. For palaeontologists, access to comparative material is important but not always practicable. The purpose of this atlas is to provide a comprehensive record of the skeletal anatomy of the Thylacine to provide researchers a useful reference for comparative studies.

Natalie M. Warburton. College of Science, Health, Engineering and Education, Murdoch University, South Street, Murdoch WA 6150, Australia. N.Warburton@murdoch.edu.au
Kenny J. Travouillon. Western Australian Museum, Locked Bag 49, Welshpool DC, WA 6986, Australia. Kenny.Travouillon@museum.wa.gov.au
Aaron B. Camens. Ecology and Organismal Biology, College of Science and Engineering, Flinders University, Bedford Park SA 5042, Australia. aaron.camens@flinders.edu.au

Keywords: Marsupialia; osteology; craniodental; postcranial; photographic

Submission: 26 November 2018 Acceptance: 25 April 2019

INTRODUCTION

Thylacines were once common across much of southern Australia and were also recorded in fossil deposits from a few sites in northern Australia (Archer, 1974; Dixon, 1989). Thylacines are also represented in rock art throughout Australia from Victoria (e.g., Gunn, 2002) to Arnhem Land and the

Warburton, Natalie M., Travouillon, Kenny J., and Camens, Aaron B. 2019. Skeletal atlas of the Thylacine (*Thylacinus cynocephalus)*. *Palaeontologia Electronica* 22.2.29A 1-56. https://doi.org/10.26879/947
palaeo-electronica.org/content/2019/2542-thylacine-skeletal-atlas

Kimberley (see Bednarik, 2013 and references therein). They disappeared from the mainland fossil record as recently as 3290±49 years BP, at approximately the same time as the Tasmanian Devil (*Sarcophilus harrisii*) (Saltré et al., 2016; White et al., 2018). This coincides with the oldest known dingo material from Australia (~3.5 ka, Macintosh, 1964; Cairns et al., 2017), though the role that the dingo may have had in the mainland extinction of these two species is poorly understood. Although there has been much conjecture about the continued existence of Thylacines on both mainland Australia and in Tasmania, the youngest verified specimen remains the individual that died in captivity at Hobart Zoo in 1936.

Evolutionary History of Thylacines

Strongly convergent morphology with South American metatherian carnivores, the borhyaenids, have previously led to hypotheses of phylogenetic affinities (Bensley, 1903; Archer, 1976). However, high degrees of convergence and homoplasy in craniodental features are problematic for morphology-based taxonomy within the order Dasyuromorphia (Wroe, 1997). The most recent molecular-based phylogenies place thylacinids as the most basal group within the Dasyuromorphia, sister to a clade including dasyurids (dunnarts, quolls, devils, etc.) and myrmecobiids (numbats) (Westerman et al., 2016; Kealy and Beck, 2017). Earlier studies based on both morphological and molecular characters suggested that the three families comprising the Dasyuromorphia (Thylacinidae, Myrmecobiidae and Dasyuridae) diverged around ~26–27 Ma (Beck, 2008; Meredith et al., 2009; Black et al., 2012). More recent work considers the divergence time to be around 40 Ma (Mitchell et al., 2014; Westerman et al., 2016; Kealy and Beck, 2017). The earliest known representative of the Thylacinidae is a fragmentary right M^2 from the late Oligocene Pwerte Marnte Marnte Local Fauna of the Northern Territory (Murray and Megirian, 2006). The age of this deposit, based on stage of evolution and biocorrelation, is thought to be slightly older than 23–25 Ma, placing it within the range of the estimated divergence date of the major dasyuromorphian clades.

The majority of fossil thylacine taxa are known from the Oligo-Miocene deposits of central South Australia, the Northern Territory and northern Queensland. Although nine genera and 14 species of thylacinid are currently recognised in the fossil record (Yates, 2015), a study by Kealy and Beck (Kealy and Beck, 2017) revealed that *Mutpuracinus archibaldi* may instead be a plesiomorphic dasyuromorphian. Thylacinids were at their most diverse during the early to middle Miocene (Wroe, 2001; Kealy and Beck, 2017); being represented by relatively few taxa from the late Miocene onwards (e.g., Dawson, 1982). The decrease in thylacinid diversity coincides with the decline in global temperature associated with the end of the Miocene Climatic Optimum and an increase in dasyurid diversity (Kealy and Beck, 2017). Recent studies have revealed greater diversity during the late Miocene/early Pliocene (Yates, 2015) but by the Pleistocene, the family was represented by the single species *Thylacinus cynocephalus*.

Brief Literature Review of Anatomy of Thylacine

Early accounts by Europeans highlighted the strong morphological and ecological convergence of *Thylacinus* on canids, especially wolves. They display an overall body shape that is quite dog-like, and the cranial shape in particular shows remarkable convergence with placental canids (see figure 3 in Warburton and Dawson, 2015).

Historically, specimens were apparently available for scientific study, with mentions of Thylacines in comparative encyclopaedic works such as those by Owen (1868). Further, more detailed studies of regional musculoskeletal and neural anatomy were performed (Cunningham, 1878a, 1878b, 1881, 1882; Thomas, 1888). We cannot, however, find an easily accessible description of the postcranial skeletal elements — and thus have herein included a brief description of each of the elements of the postcranial skeleton to highlight features that may be of interest when examining the illustrated bones.

Studies of craniodental anatomy have concluded that the thylacine had most likely taken small- to medium-sized vertebrate (principally mammalian) prey (Jones, 1997; Wroe et al., 2007) and was likely restricted to the consumption of soft-tissues. Canine cross-sectional shape was found to be similar to that of quolls, suggesting thylacines killed prey with a crushing bite (Jones, 1997). Canine bite force has been calculated to be less than that of smaller bodied Tasmanian devil (*Sarcophilus*), and the temporalis muscle is relatively smaller, suggesting thylacines took smaller prey than devils (Jones, 1997). However, the observed differences in bite force may instead be related to the relative degree of osteophagy rather than prey size. These interpretations of thylacines likely being restricted to relatively small prey have been

corroborated via three-dimensional finite element analysis, which found that the skull of *T. cynocephalus* was not particularly adapted to withstand high biomechanical forces induced by either jaw-muscles or struggling prey (Wroe et al., 2007; Attard et al., 2011). Though thylacines are recognised to have had a very wide gape among mammals, this may have been linked to agonistic behaviours and displays rather than related to the acquisition of large prey (Attard et al., 2011).

Attempts to classify the locomotor and hunting adaptations of the thylacine on the basis of comparisons with the appendicular skeleton of placental mammals generally returns a 'generalised' terrestrial verdict. On the basis of limb ratios Jones and Stoddart (1998) suggested an open habitat, pounce-pursuit hunting strategy of medium-sized prey. Detailed analysis of the articular shape of the elbow joint lead Figueirido and Janis (2011) to similarly conclude that the thylacine was not specialised for fast running but rather was most likely to have utilised ambush strategies rather than pursuit predatory behaviours. However, Janis and Figueirido (2014) refuted these previous classifications, following consideration of a greater number of forelimb elements, including linear dimensions of the scapula, humerus, ulna and radius. In that study, thylacines did not group definitively with either pounce or pursuit extant carnivorans, and were considered to be more generalised than any extant placental. This has evoked suggestions that forelimb adaptation toward cursorial specialisation in marsupials is constrained by the requirements of the neonatal crawl to the pouch (Figueirido and Janis, 2011; Janis and Figueirido, 2014; Sears, 2004) (though other marsupials do have quite dramatic modifications of the forelimb and elbow for behaviours such as digging; e.g., Warburton, 2006; Warburton et al., 2014). The studies of the functional morphology of thylacines rely on the skeletal morphology of extant placental mammals for comparison, and do not consider potential anatomical and physiological adaptations of muscles among marsupials. Without such information for the thylacine, however, these skeletal interpretations remain our best hypotheses.

Purpose and Objectives of Current Work

Despite the number of animals that were killed during the extermination of thylacines from Tasmania, very few useful specimens exist in collections. For palaeontologists, access to comparative material is important but not always practicable. The purpose of this atlas is to provide a comprehensive view of the skeletal elements of the Thylacine to enable researchers (without access to skeletal material) a useful reference for comparative studies. We have tried as much as possible to keep figures to the same scale to allow printing at life size when desired.

MATERIALS AND METHODS

Cranial terminology follows Wible (2003), and dental terminology follows Wroe and Musser (2001). Postcranial terminology primarily follows Miller's Anatomy of the Dog (Miller, 1979). Descriptions pertain to the individual specimens figured and many features are likely to exhibit intraspecific variation to some degree.

Specimens

SAMA M1960 (the main skeleton photographed for the atlas) was a specimen that died in captivity at the Adelaide Zoo (date unknown, unknown sex, stored in the South Australian Museum).

SAMA M95 (thoracic vertebrae featured in atlas) was a large adult male individual supplied to the South Australian Museum (SAM) by A. McGowan on the 12 July 1912 from Tasmania. Both the skin and skeleton are deposited in the SAM. It seems likely that this was Mr. William McGowan, the Superintendent of Public Reserves at the Launceston City Park (1882–1937) who ran "a flourishing export business in Thylacines" (Sleightholme and Ayliffe, 2013, p. 106). With the exception of a few pouch young, all specimens McGowan exported were wild-caught, so it is most likely that SAMA M95 was also a wild-caught specimen.

SAMA M665/001 is a mounted skeleton stored in the South Australian Museum, from which the chevron bones were recovered.

WAM M195 (incorrectly labelled WAM M3318, see below) from which the photographs of the adult skull were taken is a mounted skeleton of unknown sex (disarticulated to photograph, stored in the Western Australian Museum).

WAM M17189 (used here for the dental description) is a juvenile female, skin and damaged skull, from Hobart Museum 1896 (stored in the Western Australian Museum).

About M195 and M3318: The mounted skeleton was found by W.D.L. Ride in 1957 in the WA Museum collection without any registration number or data. He registered it as M3318 and noted in the remarks field of the catalogue that this specimen is "Possibly the same as M195, an untraced skeleton

from Hobart, A.J. Taylor Sept 29th 1914. O. Lipfert does not appear to have made this skin (K.G. Buller). Glauert says that he understood that this is the skeleton of skin no. 58, which was presented by Hobart Museum, but that specimen arrived before his time. Skull, Skeleton (skin on display — AM Douglas January 1975)." Upon further research, we found that two specimens of *Thylacinus cynocephalus* were purchased from the Curator of "The Museum" in Hobart on April 9, 1896 and sent by Alexandre Morton in September 1897 to the Western Australian Museum. One of these specimens was registered in the old Museum catalogue as number 58 by L. Glauert as a male specimen from Hobart Museum, Tasmania, April 1896. This specimen matches a taxidermy with the same number attached to its leg and is indeed a male. The second specimen was registered later as WAM M17189 (used here for the dental description), a juvenile female, skin and skull, from Hobart Museum 1896. Its old accession number '2/0138' did not match any catalogue entries. We found in the Museum Archives a series of letters between the WA Museum (then known as the Perth Museum) director, B.H. Woodward and the director of the Tasmanian Museum in Hobart, G.H., Hardy that helped to untangle the origin of each thylacine specimen. In the first letter dated September 19, 1913, Woodward asked Hardy if he had any skeletons of the Tasmanian Wolf or Tiger for an exchange, as he was very anxious to have one to compare with the fossil remains found in WA (which L. Glauert was collecting from the south west of WA). This information suggests that in 1913, there was no thylacine postcranial material in the WA Museum. The exchange of letters continued until the March 10, 1914. To summarize these exchanges, the Tasmanian Museum, having only one skull and one skeleton in its collection, was not able to part with any specimen. Despite their unsuccessful efforts to acquire more specimens from the wild, the Tasmanian museum could not acquire any new specimen for the WA Museum, and due to the high demand of access to the specimens in their collection, the Tasmanian Museum could not loan any of them to the WA Museum. While there are no subsequent correspondences on the thylacine in the WA Museum archive, the first mammal catalogue of the WA Museum shows that on September 29, 1914, the WA Museum acquired a thylacine skeleton from Mr. A.J. Taylor, from Hobart, Tasmania, registered as WAM M195. We have since X-rayed the taxidermy acquired in 1897 (old catalogue number 58) and found that a skull is present, and therefore it cannot be the same individual as the skeleton M195 (which also includes a skull). Considering the evidence presented and timeline, it is therefore impossible that the skeleton registered by Ride as WAM M3318 is the same individual as the taxidermy numbered 58. The skeleton is therefore specimen WAM M195, while taxidermy number 58 will remain as specimen WAM M3318. As a result, the WA Museum has three modern *Thylacinus* specimens, instead of two, which will be of interest to many researchers who have used the WA specimens in the past and of interest to the International Thylacine Specimen Database (Sleightholme and Campbell, 2018).

WA Museum specimens were photographed using a Hasselblad H4D camera, on a camera stand. SA Museum specimens were photographed using a Canon EOS 700D and tripod.

For reference, we have provided a table of basic measurements of the skeletal elements (Table 1).

DESCRIPTIVE ANATOMY

Craniodental

The craniodental description is principally based on specimen WAM M195 (incorrectly labelled WAM M3318, see above), with occasional reference to a juvenile specimen WAM M17189 in regard to dental wear.

Facial skeleton (Figures 1-6). The rostrum is long and narrow compared to other dasyuromorphians (Wroe and Milne, 2007), with the narrowest point being level with the anterior of P3 (in ventral view). In dorsal view, the nasal bones are narrow anteriorly and widen posteriorly in the last third of their lengths. The nasals do not extend as far as the anterior border of the premaxilla; rather their anterior margin is level with the midpoint of the incisive foramina. In anterior view, the nares are ovoid, only just taller than they are wide. In lateral view, the premaxillary-nasal suture is as long as the maxillary-nasal suture but shorter than the premaxillary-maxillary suture. The anterior limit of the facial process of the premaxilla is rounded. The premaxilla houses four uni-rooted incisors (I1-4) followed by a sulcus to accommodate the tip of the lower canine (c1) when the jaws are closed. The premaxilla borders the upper canine root (C1) anteriorly and medially, while the maxilla borders it laterally and posteriorly. The maxilla houses three double-rooted premolars (P1–3) and four triple-rooted molars (M1–4). Two short diastemata are present

TABLE 1. Standard measurements of WAM M195, SAMA M11960, M95, in mm.

Specimen Element Measurement	WAM M195		SAMA M11960		SAMA M95	
Skull						
Length (max.)	224		214		255	
Width (max.)	125.3		117.3		143.3	
Dorsoventral height (max.)	72		75		84	
Tooth row length (max.)	110.8		109		124	
Length molar row	46.06					
Dentary						
Length (max.)	181.2		177.1,	178.2	210	210
Dorsoventral height (max.)	63.2		72,	68	77.3	79
Width (max.)	31.8		33.3,	30.1	45.6	44
Tooth row length (max.)	108.2		104.6,	104.4	121.2	120
Length molar row	49.8					
Scapula						
dorsventr L	138.7,	139.6	139.5,	140.9	165.5	~165
crancaud L	64.2,	63.15	70.3,	69.44	88	84
glenoid fossa L	27.3,	28	24.,3	24.9	29.5	28.1
glenoid fossa w	18.3,	17.9	17.0,	17.7	18.9	20.5
L neck	24.8,	23.3	23.7,	23.4	28.6	27.8
L scapular spine (incl acromion)	126.3,	124.2	128.4,	127.2	148.9	150.3
Clavicle						
Length (max.)	N/A	N/A	N/A	N/A	40.1	42.2
Width (max.)	N/A	N/A	N/A	N/A	11.2	10
Humerus						
Length (max.)	162,	163	159.4,	161.8		184.1
Width (max.) proximal	32.6,	30.9	27.5,	26.9		31.6
Craniocaudal depth (max.) proximal	43.9,	42.3	39.8,	40.2		46.7
Width (max.) distal	30.8,	29.4	28.5,	28.3		33.6
dist depth	19.2,	-	18.7,	19.2		20.7
width trochlea + capitulum	24.6,	24.8	23.2,	22.6		27.5
Ulna						
Length (max.)	189,	190	188.6,	188.9		
Olecranon length (from mid-trochlear notch)	35.3,	35.4	32.3,	33.3		
Olecranon depth (max.)	19.4,	17.6	17.5,	17.9		
Width (max.) distal	13.1,	16.8	9.9,	9.2		
Craniocaudal depth (max.) distal	16.2,	14	14.0,	13.4		
Radius						
Length (max.)	154.2,	153	156.7,	156.7		
Width (max.) proximal	15.3,	14.3	13.8,	14.1		
Craniocaudal depth (max.) proximal	11.6,	11.5	10.4,	10.6		
Width (max.) distal	16.7,	16.5	16.7,	16.2		
Craniocaudal depth (max.) proximal	12.9,	13.3	11.7,	13.8		

TABLE 1 (continued).

Specimen Element Measurement	WAM M195		SAMA M11960		SAMA M95	
Metacarpal I						
Length (max.)	19.1,	19.2	16.5,	17.1		
Width (max.) distal	7,	7.5	6.9,	7		
Metacarpal II						
Length (max.)	36,	35.5	36,	36.4		
Width (max.) distal	9.3,	8.5	9.3,	9.8		
Metacarpal III						
Length (max.)	40.9,	39.7	40.3,	40.7		
Width (max.) distal	9.3,	9.4	9.4,	9.5		
Metacarpal IV						
Length (max.)	40.5,	39.2	38.9,	40.1		
Width (max.) distal	9.6,	9.3	10.1,	10.2		
Metacarpal V						
Length (max.)	27.6,	27.2	27.9,	28.1		
Width (max.) distal	8.9,	8.6	8.9,	8.8		
Pelvis						
Length (max.)	156.3,	157.3	161,	160	182.6,	183.5
Width (max.) across ilia	90.3		92			112.3
Width (max.) across ischia	75.1		76.8			84.4
Ilium length (from mid-acetab.)	87.4		87.1,	88.7	101.7,	103.8
Pelvic symphysis length	72.2		78.7		82.3,	
Femur						
Length (max.)	192.8,	193	189.8,	190.7	212,	212
Width (max.) proximal	39.5,	39.7	39.3,	39.6	44.9,	44.3
Craniocaudal depth (max.) proximal	21.6,	23.3	24.7,	24.4	26,	24.5
Width (max.) distal	30.8,	30.6	30.2,	30.2	33.6,	34.3
Craniocaudal depth (max.) distal	28.1,	28.4	27.3,	26.7	31.2,	30.7
Midshaft diameter (med-lat)	14.2,	14.5	14.4,	15.0	15.8,	15.5
Tibia						
Length (max.)	187,	185	185.7,	184.9		
Width (max.) proximal	29.3,	29.8	29,	29		
Craniocaudal depth (max.) proximal	34.4,	31.3	32,	32		
Width (max.) distal	16.6,	17.1	16,	17.2		
Craniocaudal depth (max.) distal	19.3,	17.2	18.9,	18		
Fibula						
Length (max.)	178,	179.7	178.7,	178.4		
Width (max.) proximal	8.7,	10.3	9.5,	9.1		
Craniocaudal depth (max.) proximal	17,	17.1	17,	16.5		
Calcaneus						
Length (max.)	40.9,	41.9	39.6,	39.7		
Width (max.)	18.4,	18.1	17.8,	18.4		
Dorsoventral height (max.)	16.1,	15.2	15.5,	17.7		

TABLE 1 (continued).

Specimen Element Measurement	WAM M195		SAMA M11960		SAMA M95
Talus					
Length (max.)	16.8,	18.2	18.5,	17.5	
Width (max.)	18.7,	18	19.5,	19.1	
Dorsoventral height (max.)	12.4,	10.8	11.2,	11.3	
Cuboid					
Length (max.)	8.7,	11.5	10.9,	10.8	
Width (max.)	15.5,	17.6	18.1,	17.1	
Dorsoventral height (max.)	15.8,	16	15,	15.4	
Navicular					
Length (max.)	17.5,	16.3	16.2,	16.4	
Width (max.)	13.9,	13.3	11.8,	10.5	
Dorsoventral height (max.)	12.6,	11	12.7,	12.7	
Metatarsal II					
Length (max.)	54.4,	54	54.3,	53.9	
Width (max.) distal	9,	8.7	9,	9.5	
Metatarsal III					
Length (max.)	58.7,	60.5	59.4,	58.2	
Width (max.) distal	9.9,	9.6	9.8,	10	
Metatarsal IV					
Length (max.)	59.8,	59.7	60.3,	60.2	
Width (max.) distal	9.2,	10.2	9.4,	9.4	
Metatarsal V					
Length (max.)	50.8,	54.7	54.7,	52.6	
Width (max.) distal	8.5,	8.4	10.4,	9.1	

between P1 and P2, and P2 and P3. The very large infraorbital foramen is present on the maxillary-jugal suture. The infraorbital canal is very short and ends below the orbit. A small foramen is present below the infraorbital foramen. The transition between the maxilla and the jugal (zygomatic) is smooth, with no distinct antorbital fossa. About a third of the lacrimal extends out of the orbit and onto the facial region, where it is bordered by the frontal dorsally, maxilla anteriorly, and jugal ventrally. Lacrimal foramina are variable; there are two lacrimal foramina (one large ventral foramen and one small dorsal foramen) on left side of the skull, and a single large lacrimal foramen on the right side of the skull. These lacrimal foramina are posterolaterally directed. Another small foramen is present dorsal to the lacrimal foramina within the lacrimal bone, and this foramen is anterodorsally directed. The facial portion of the lacrimal is separated from the neurocranium by a very well-developed lacrimal crest that lines the anteromedial portion of the orbit. The anterior portion of the frontal is flared, projecting laterally as a distinct postorbital process.

Neurocranium (Figures 1-5). The posterior margins of the lacrimal are shared with the frontal dorsally and palatine ventrally. Just above the lacrimal-palatine suture, the lacrimal is curved and forms a ledge around the maxillary foramen (the posterior opening of the infraorbital canal). The maxillary foramen is therefore bordered by the lacrimal dorsally, the palatine medially, the maxilla ventrally, and the jugal laterally. Posterior to the maxillary foramen, a large and ovoid sphenopalatine foramen is present and completely enclosed by the palatine. Posteriorly, the palatine is bordered dorsally by the frontal and posteriorly by the alisphenoid, and it extends as far back as the sphenorbital fissure. The sphenorbital fissure is large and ovoid in shape. It is principally bordered by the

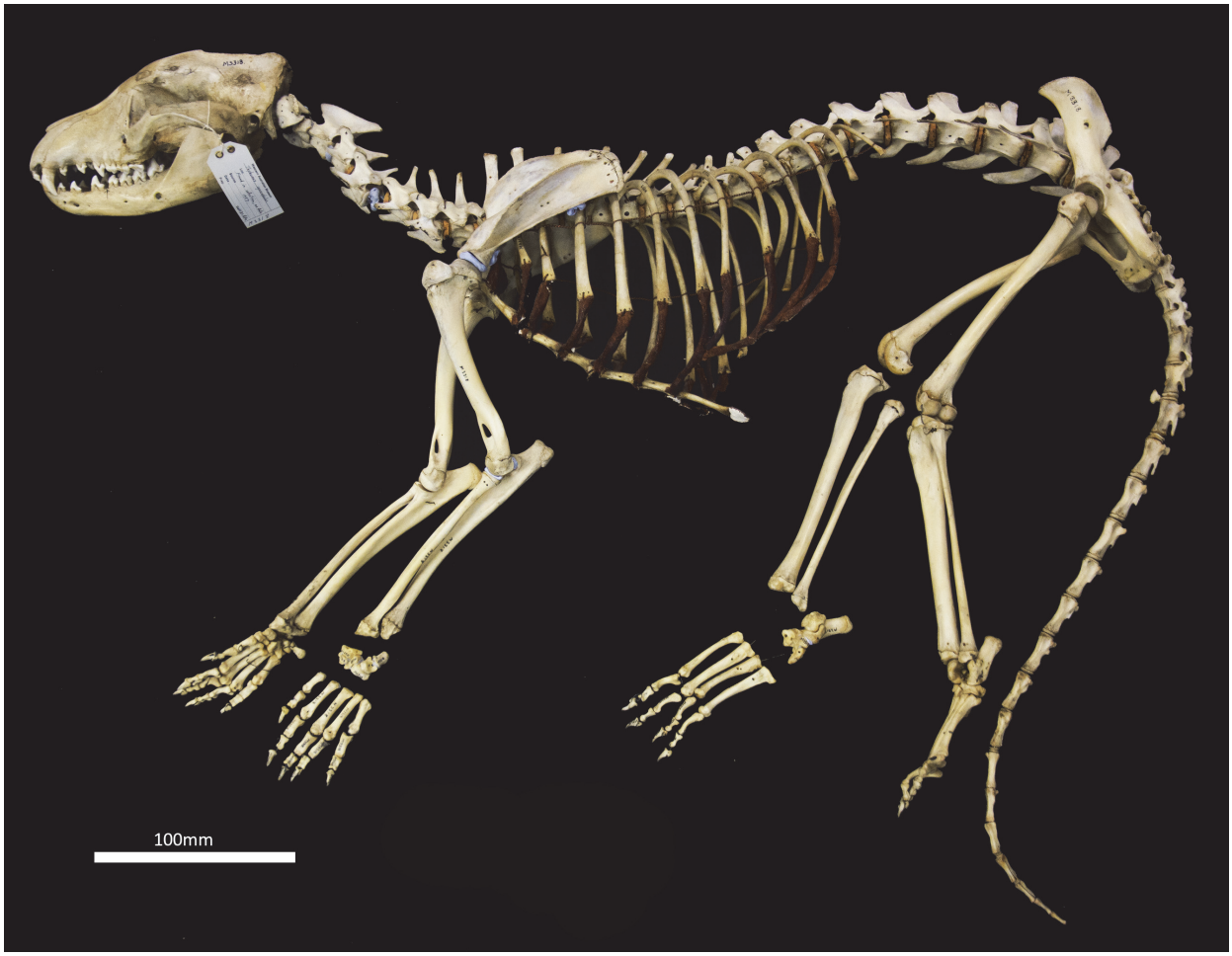

FIGURE 1. Thylacine skeleton, WAM M195 (M3318).

alisphenoid, except for the medial wall, which is formed by the orbitosphenoid. The ventral surface of the sphenorbital fissure is crested, at the junction between the alisphenoid and orbitosphenoid. The orbitosphenoid is quite large, and extends anteriorly to form the lateral wall of the ethmoidal foramen. This small ovoid and anteriorly directed foramen is otherwise bordered by the frontal. Posterior to the sphenorbital fissure, the small and circular foramen rotundum is anteriorly directed and completely enclosed within the alisphenoid. Ventral to the sphenorbital fissure, the pterygoid canal is small, round and anteriorly directed. The alisphenoid extends upward toward the parietal, but it is completely surrounded anteriorly and dorsally by the frontal, and posteriorly by the squamosal. In dorsal view, the frontals narrow posteriorly from the postorbital process. Medially, the frontals form V-shaped crests that merge posteriorly to form a tall sagittal crest. The sagittal crest continues posteriorly through the parietals and interparietal, forming the medial wall of the temporal fossa. Sutures close to the sagittal crest are fused and, as a result, the frontoparietal (or coronal) suture is only visible 10 mm away from the sagittal crest. This suture is short and posteroventrally directed. The parietosquamosal suture is anteriorly convex and posteriorly concave. The parietointerparietal suture is jagged. The interparietal flares posterolaterally, against the supraoccipital to form the nuchal crest; in the mid-sagittal line it contributes to the posterior-most section of the sagittal crest. Ventral to the interparietal, the petrous portion of the squamosal contributes to the neurocranium. The squamosal (temporal) contributes to the posterolateral walls of the neurocranium and extends anterolaterally to form the posterior portion of the zygomatic arch. The large external auditory meatus is visible laterally and is almost completely walled by the squamosal, except for the ventral side, which is walled by the ectotympanic. Dorsal to the external auditory meatus is the smaller, ovoid and posterolater-

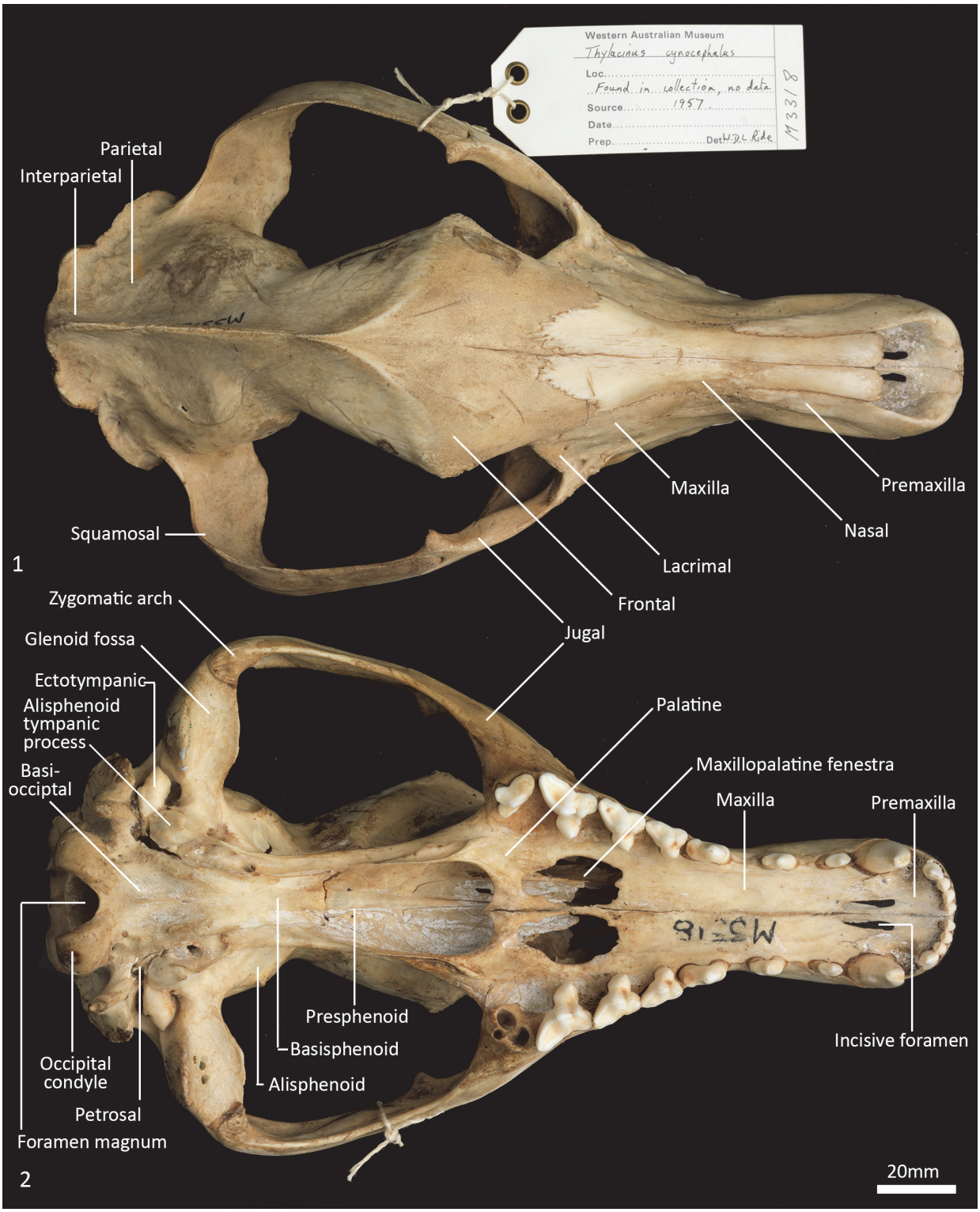

FIGURE 2. Skull of WAM M195 (M3318). **1,** dorsal view; **2,** ventral view. Scale bar equalsequals 20 mm.

FIGURE 3. Juvenile damaged skull of WAM M17189. **1,** dorsal view; **2,** ventral view. Scale bar equals 20 mm.

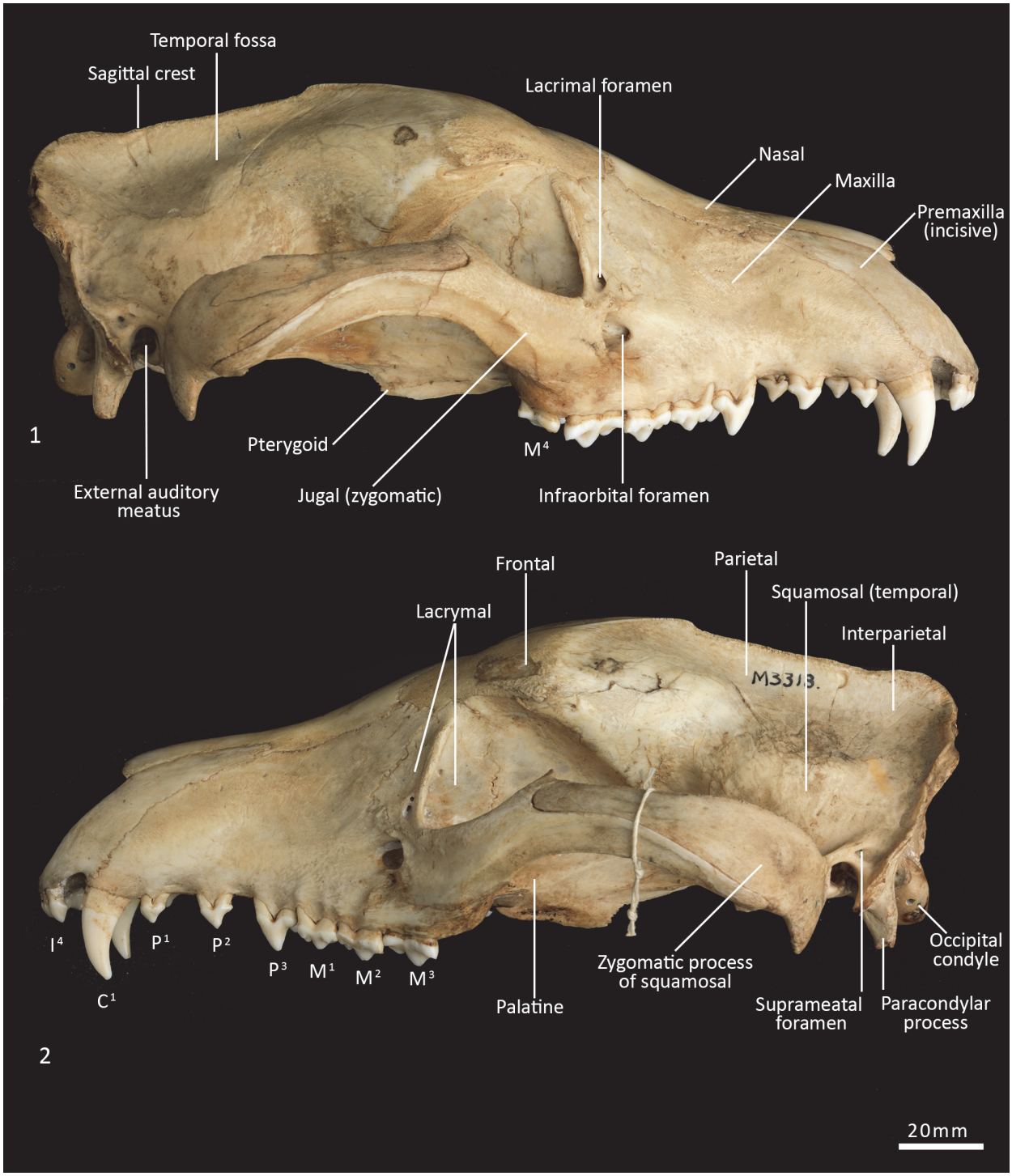

FIGURE 4. Skull of WAM M195 (M3318). **1,** right lateral view; **2,** left lateral view. Scale bar equals 20 mm.

FIGURE 5. Juvenile damaged skull of WAM M17189. **1,** right lateral view; **2,** left lateral view. Scale bar equals 20 mm.

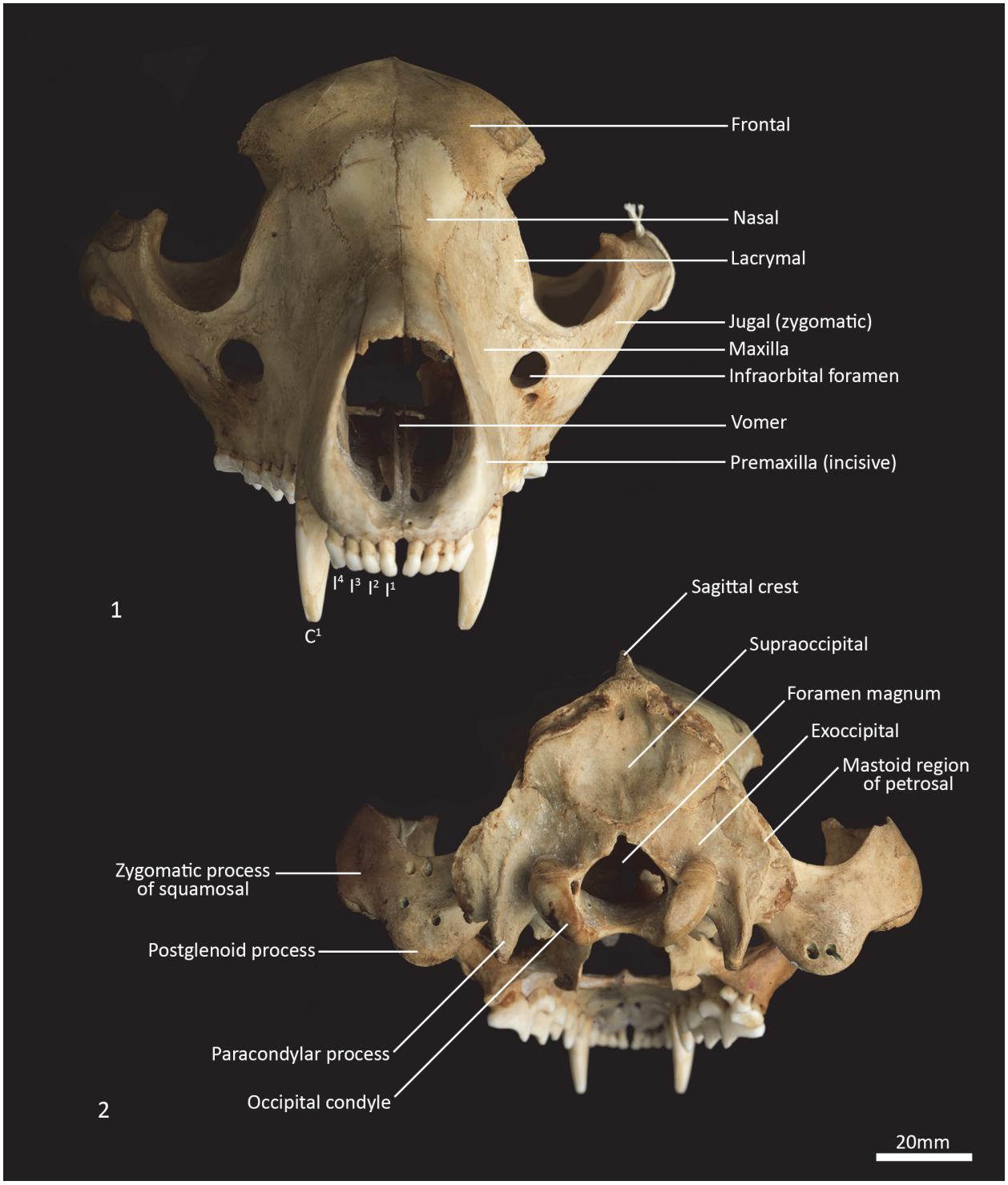

FIGURE 6. Skull of WAM M195 (M3318). **1,** rostral view; **2,** caudal view. Scale bar equals 20 mm.

ally directed suprameatal foramen. The zygomatic arch is broad, and the squamosal-jugal suture is long and deep. The jugal contributes to the ventral surface of the zygomatic arch posteriorly, to level with the glenoid fossa, and has an obvious masseteric line arching along its length. A distinct postorbital process is present on the dorsal surface of the jugal at the U-shaped jugosquamosal suture.

Palate (Figures 2-3, 7). In ventral view, the maxillopremaxillary suture is V-shaped. The paired incisive foramina are moderately long and very narrow. They are bordered by the premaxilla anteriorly and medially and the maxilla laterally and posteriorly. There are no additional fenestrae between the incisive foramina and the maxillopalatine fenestrae. In this region, the palate is mostly flat, rising only slightly at the intermaxillary suture. There are two deep sulci between M2 and M3, and M3 and M4. The maxillopalatine fenestrae are somewhat ovoid in shape with irregular margins and are separated by a thin central septum. They extend anteriorly level with the protocone of M2, and posteriorly with the anterior of M4. The anterior two-thirds of the maxillopalatine fenestrae are bordered by the maxilla, and the posterior third are bordered by the palatine. The postpalatine torus is curved and heavily thickened. There are no distinct minor palatine foramina. Posteriorly, the palatine and the pterygoid sutures are obliterated. The pterygoid thins posteriorly to a thin blade of bone that forms the lateral wall of the nasopharyngeal passage.

Cranial floor (Figures 8-9). In ventral view, the presphenoid forms the roof of the nasopharyngeal passage. It is shaped as an anteriorly directed and very long isosceles triangle, bordered first anteriorly by the palatine, then by the pterygoid. Its posterior margin contacts the hourglass-shaped basisphenoid. Just lateral to this contact is the exit of the pterygoid canal. The basisphenoid is met laterally by the alisphenoid that contributes to the posterior portion of the lateral walls of the nasopharyngeal passage. Posteriorly, the basisphenoid flares laterally to meet the basioccipital. The posterior third of the basisphenoid is marked by a distinct lateral crest. The basisphenobasioccipital suture is fused. Just lateral to this suture is the carotid foramen, which is posterolaterally directed and completely walled by the alisphenoid. Anterior to the carotid foramen is the transverse sinus canal, which is bilaterally asymmetric in this specimen; on the left side, it is just anterior to the carotid foramen, but on the right side, it is much more anteriorly positioned, level with the midpoint of the basisphenoid. The opposite (i.e., more anterior position on the left side) is seen in WAM M17189. A small ovoid foramen is present on the basioccipital, immediately posterior to the basisphenobasioccipital suture. Posterior to this foramen is a central crest, which ends just as the basioccipital curves ventrally toward the foramen magnum. Laterally, two pairs of hypoglossal foramina are present on either side of, and just anterior to, the occipital condyles. Anterolateral to the hypoglossal foramina, the foramina for the inferior petrosal sinus (medial) and the jugular foramen (lateral) are separated by small processes of the exoccipital and petrosal. In WAM M17189, these two processes contact each other, separating the foramen of the inferior petrosal sinus from the jugular foramen. Very little of the petrosal is visible in ventral view, except for the long crested rostral tympanic process. Anterior to the petrosal, the foramen for the greater petrosal nerve is present as a long, narrow opening. Just lateral to this foramen is the groove for the auditory tube, which is lined medially by the petrosal, and dorsally and laterally by the alisphenoid. Anterior to the auditory tube, the foramen ovale is large and round. A bridge of alisphenoid is present anterolaterally to the foramen ovale, which some have interpreted to form the anterolaterally directed secondary foramen ovale (Wroe and Musser, 2001). From this bridge, the anterior part of the alisphenoid tympanic process is crested and then flattens posterodorsally. It overlaps with the medial end of the ectotympanic. The ventral surface of the ectotympanic is quite rounded, but it extends laterally and narrows down to a point against the posterior wall of the postglenoid process. Anterior to the ectotympanic, the postglenoid foramen is subdivided into two foramina by a posteriorly directed process on the alisphenoid. Within the external auditory meatus, on the right side of the skull, the malleus and incus are preserved but these are still covered with dried soft tissues, preventing an accurate description of their shape. The glenoid fossa is twice as wide as it is long, with a tall and rounded postglenoid process lining it posteriorly.

Posterior cranial wall (Figure 6). The posterior wall of the cranium is roughly triangular in shape. The dorsal half of the cranial wall is made up of the supraoccipital, which is wider than it is high. The supraoccipital is concave and flares posterodorsally. Its ventral border has a short contact with the paired petrosal (mastoid) laterally, and a long contact with the paired exoccipitals medially. A single foramen is present in the dorsal half of the supraoccipital, roughly in its centre. The petrous portion

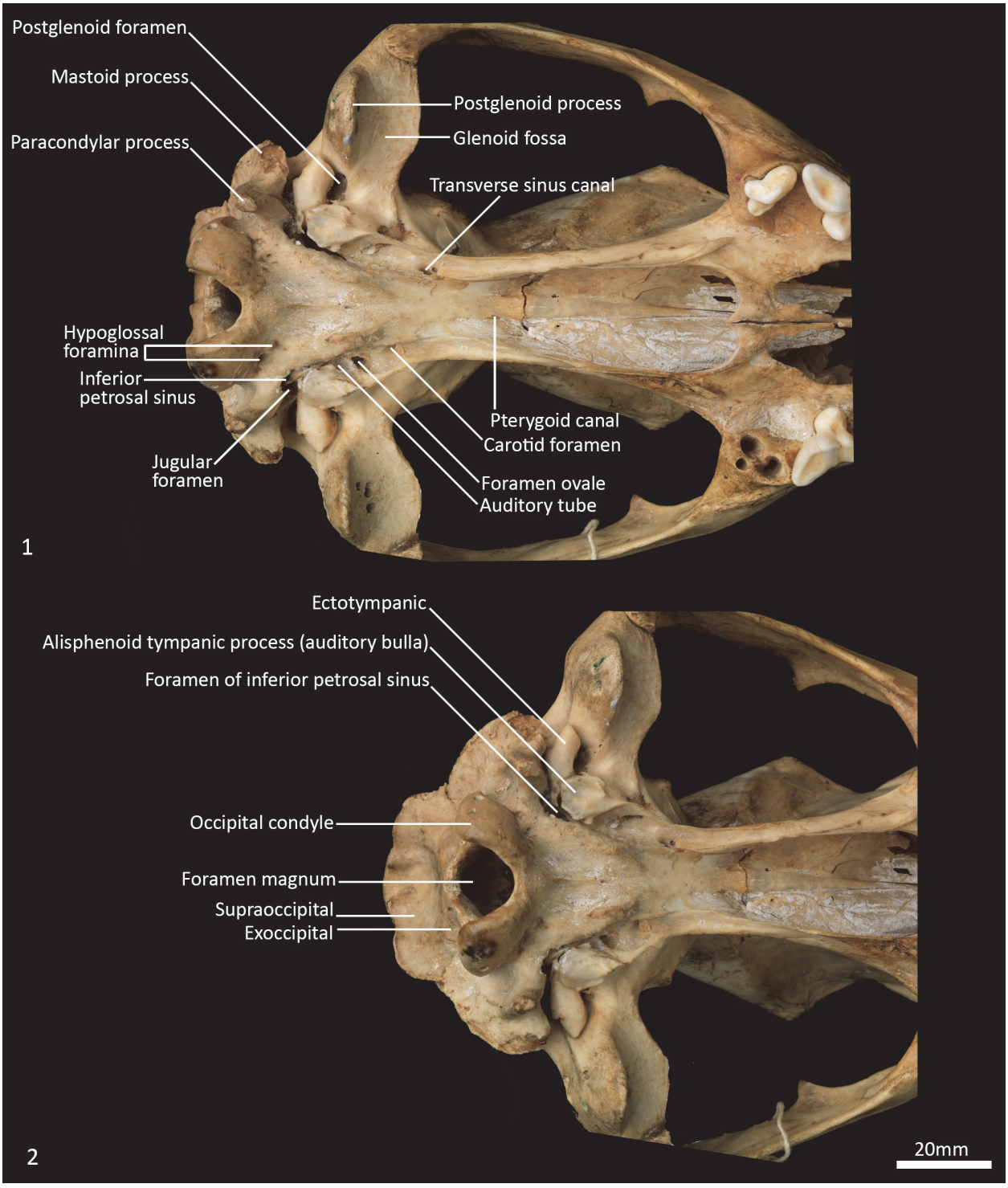

FIGURE 7. Features and foramina of skull WAM M195 (M3318). **1,** ventral view; **2,** caudoventral view. Scale bar equals 20 mm.

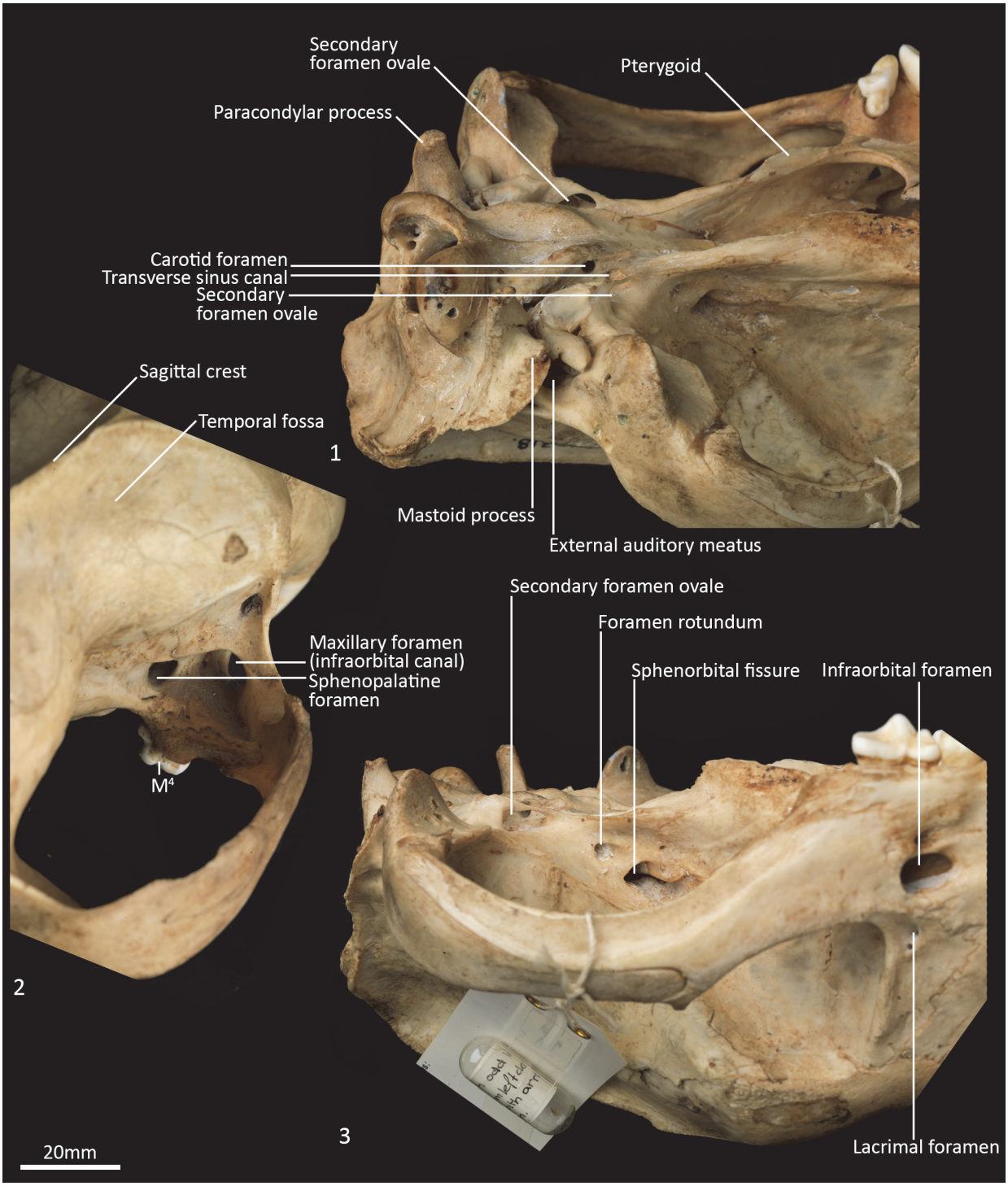

FIGURE 8. Features and foramina of skull WAM M195 (M3318). **1,** ventrolateral view; **2,** dorsolateral view of rostral orbit; **3,** lateral view. Scale bar equals 20 mm.

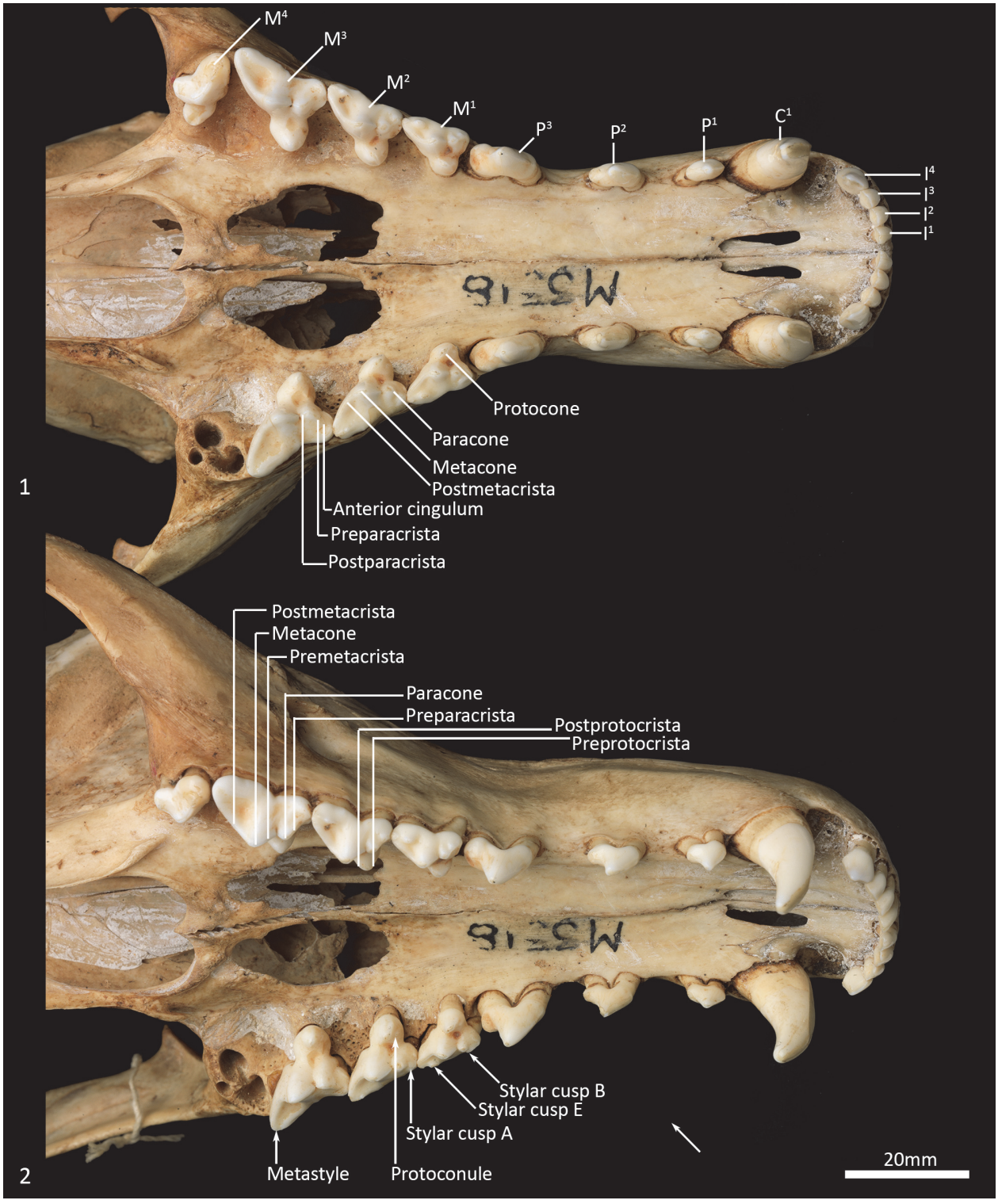

FIGURE 9. Upper dentition of WAM M195 (M3318). **1,** ventral view; **2,** ventrolateral view. Scale bar equals 20 mm. C^{1}, upper canine; I^{1-4}, upper incisor 1 to 4; M^{1-4}, upper molar 1 to 4; P^{1-3}, upper premolar 1 to 3.

of the squamosal flares laterally and contributes to the lateral side of the paracondylar process. The exoccipital contributes the remainder of the paracondylar process. The exoccipital borders the dorsal margin of the foramen magnum and surrounds the dorsal and lateral edge of the occipital condyle. The foramen magnum is roughly circular in shape. At the junction of the exoccipital and the occipital condyle is a small, circular, anteriorly directed foramen for the hypoglossal nerve. The occipital condyles are large and ovoid, and border the lateral and ventral sides of the foramen magnum.

Mandible (Figures 10-13). The mandible houses three incisors (i1–3), a canine (c1), three premolars (p1–3) and four molars (m1–4). The mandibular symphysis extends from between the roots of the incisors to the level of the anterior end of p3. There are short diastemata between p1–2, p2–3 and p3–m1. In lateral view, the mandibular corpus is curved anteriorly. It gently increases in height posteriorly until it reaches the ascending ramus. There are between two and four mental foramina on the mandibular corpus: in M195 there is one small foramen below the root of p1, one large below the p2, one small one below the diastema of p2 and p3 (only present on the left side of the dentary) and one large below the anterior root of m2. The ascending ramus departs from the mandibular corpus at an angle of 120 degrees. A distinct coronoid crest is present on the anterolateral surface of the ascending ramus, marking the anterior margin of the masseteric fossa. Lateromedially, the coronoid process is flat. The apex of the coronoid process is broad, rounded and posteriorly directed. The mandibular condyle is short, but very wide (3 ½ times the length). The angular process is wide, posteromedially directed and has a distinct dorsomedial crest. The mandibular foramen is present on the lingual side of the mandible and looks like an inverted 'L' in lingual view. The masseteric fossa is poorly developed, but the posterior shelf of the masseteric fossa is wide and deep, with a distinct dorsolateral crest.

Upper dentition (Figures 2-3, 7). I^{1-3} are similar in shape and size. They are spatulate, unirooted and unicuspid teeth. I^2 is only slightly larger than I^1, and I^3 slightly larger than I^2. In buccal view, the crown of I^{1-3} curves posteroventrally. In the juvenile (WAM M17189), the crown has a single central cusp, with a medial and a lateral crest on either side of it. As the tooth wears down (WAM M195), the central cusp levels down, and the two crests fuse to form a single lateromedially directed horizontal crest. An ovoid wear facet revealing some dentine is present on the lingual facet of these teeth. I^4 is much larger than $I^{1–3}$, almost twice as long, but about 30% wider and taller. The tall central cusp has an anteromedially directed crest, and posterolaterally directed crest. The posterior crest is longer and steeper than the anterior crest. In the juvenile, the central cusp is slightly taller than in the adult, and a wear facet seems to be present only along the two crests, with dentine exposed along the crests.

C^1 is unicuspid and very large, about three times the height of, and twice as long and wide as, I^4. The crown is strongly recurved posteroventrally. In the juvenile, there are no crests on either side of the central cusp, but in the adult, there are two distinct wear facets on the anterior side of the tooth, one directly anterior, and the other closer to the tip of the crown, though no dentine is exposed. When the lower jaw is articulated, the tip of C_1 comes in contact with the anterior wear facet, which is probably the result of tooth-on-tooth wear. The wear facet closer to the tip is therefore more likely the result of tooth-on-food wear.

P^1 is double rooted, transversely compressed and roughly triangular in lateral view. The central cusp is tall, with an anterior crest descending the crown, and a steeper and recurved posterior crest that ends at a poorly developed heel. Dental wear only occurs on the tip of the central cusp. P^2 is similar to P^1 except as follows: the tooth is larger in all dimensions, and dental wear occurs along both the anterior and posterior crests. P^3 is similar to P^2 except as follows: the tooth is larger in all dimensions, and the heel is more developed with a slight posterior cusp.

M^1 is roughly triangular in shape in occlusal view, triple rooted and longer than it is wide. The metacone is the tallest cusp on the crown, followed in decreasing order by the paracone, stylar cusp E, stylar cusp B, metastyle, protocone and protoconule. The paracone is conical and connected to stylar cusp B anterobuccally by the preparacrista. Stylar cusp B is ovoid and poorly developed, from which a crest continues anteriorly to the small anterior cingulum (a small shelf on the anterior margin of the tooth). There are no other cusps or crests on the parastylar shelf. The metastylar shelf, directly posterior to the parastylar shelf is dominated by a large conical metacone. The postmetacrista descends the posterior flank of the metacone and then curves buccally to end at the metastyle. Just anterior to the metastyle is a small conical stylar

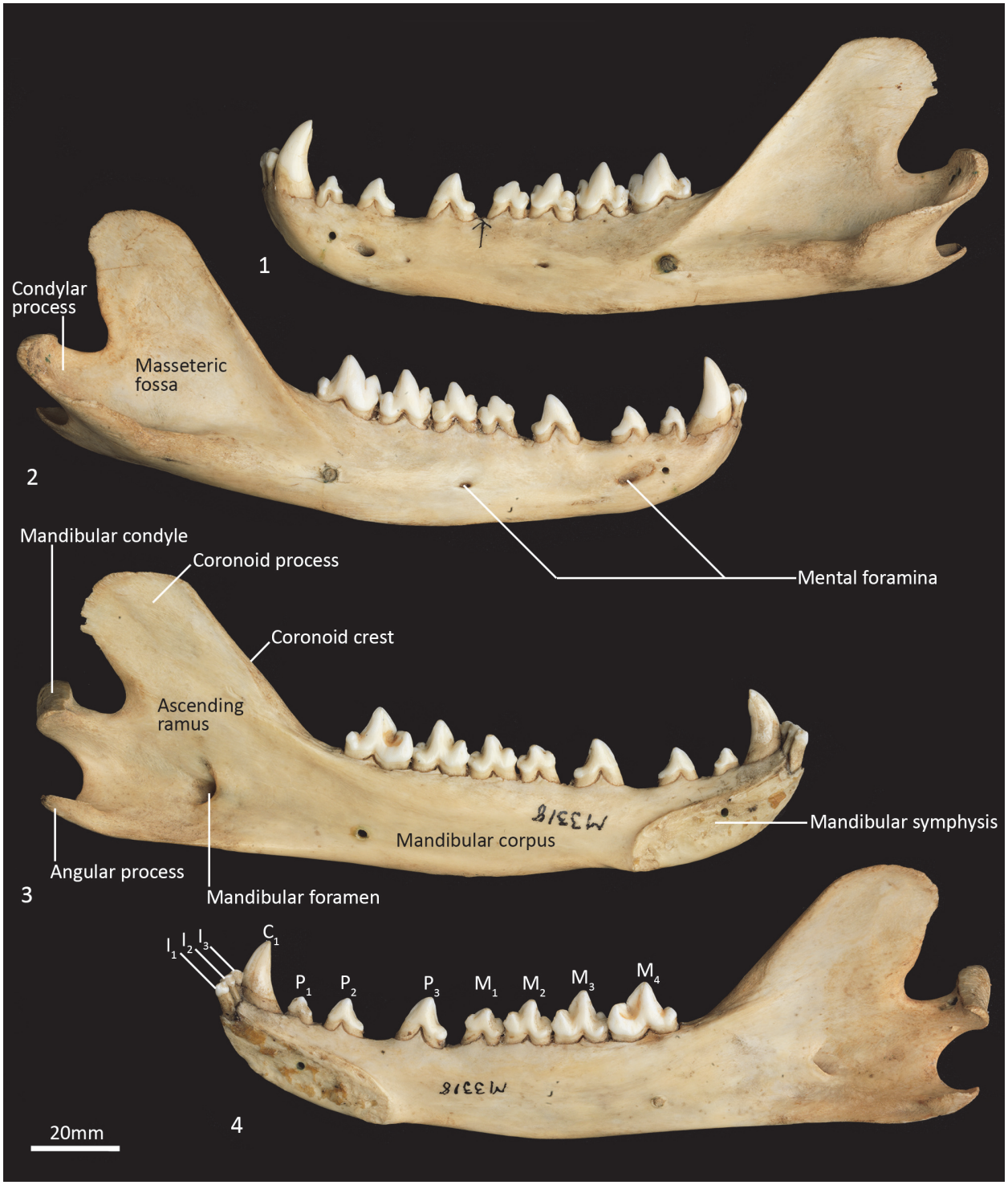

FIGURE 10. Mandible of WAM M195 (M3318). **1,** left lateral view; **2,** right lateral view; **3,** left medial view; **4,** right medial view. Scale bar equals 20 mm.

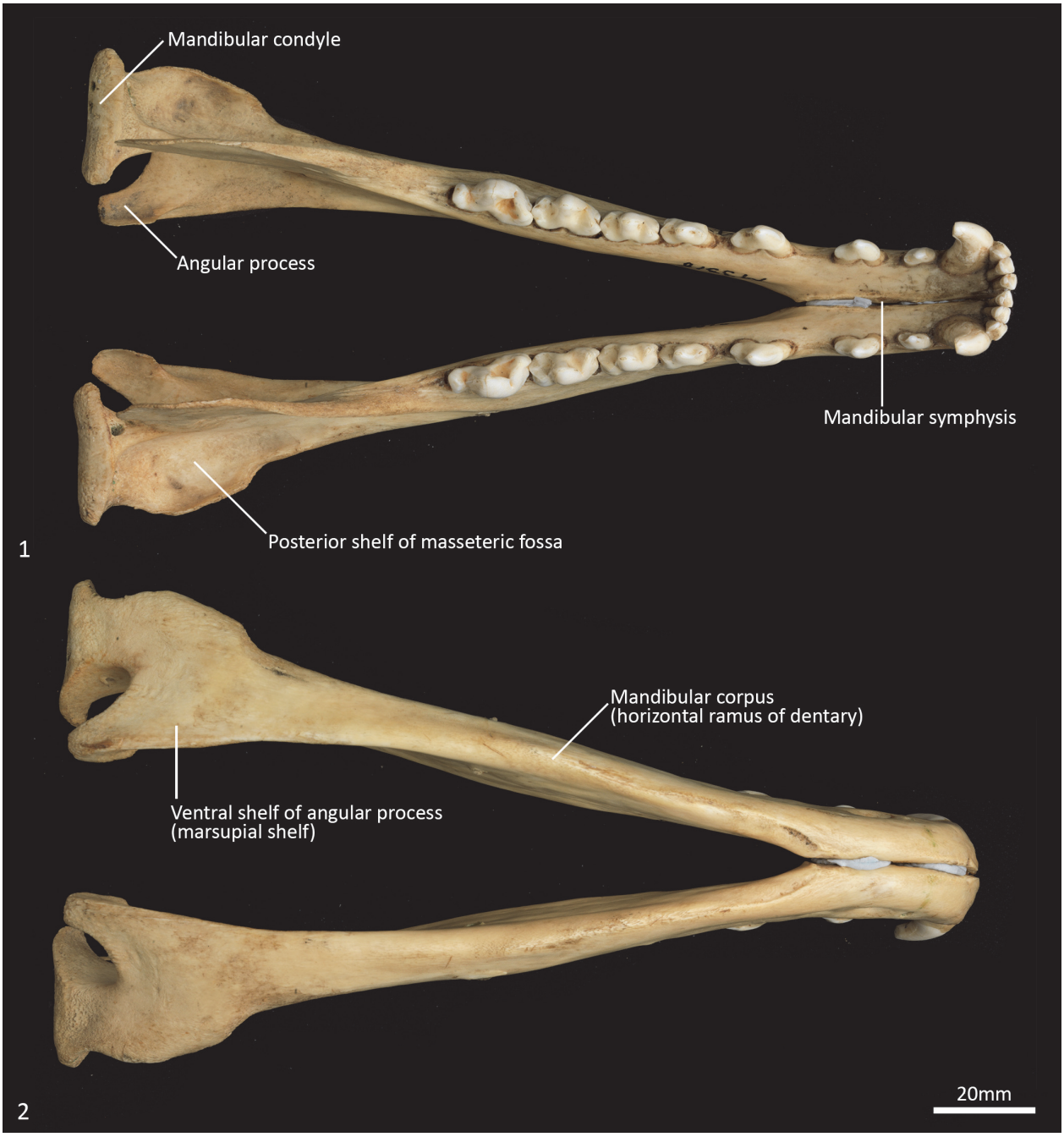

FIGURE 11. Mandible of WAM M195 (M3318). **1,** dorsal view; **2,** ventral view. Scale bar equals 20 mm.

cusp E. No other crest or cusp is present on the metastylar shelf. The trigon sits lower and lingual to the parastylar shelf and metastylar shelf. The protocone dominates the trigon and is conical. A minute conical protoconule is present anterior to the protocone. No other crest or cusp is present on the trigon. Dental wear occurs along the postmetacrista, and at the tips of the metacone, paracone, stylar cusp E, metastyle and protocone.

M^2 in comparison to M^1 is larger in all dimensions. The preparacrista joins to stylar cusp A (this cusp is not present on the M^1) anterior to stylar cusp B, and an additional crest descends anteriorly from stylar cusp B to meet the preparacrista at stylar cusp A; a postparacrista descend the posterior side of the paracone and meets a premetacrista in the valley; a premetacrista is present on the anterior flank of the metacone; stylar cusp E is reduced

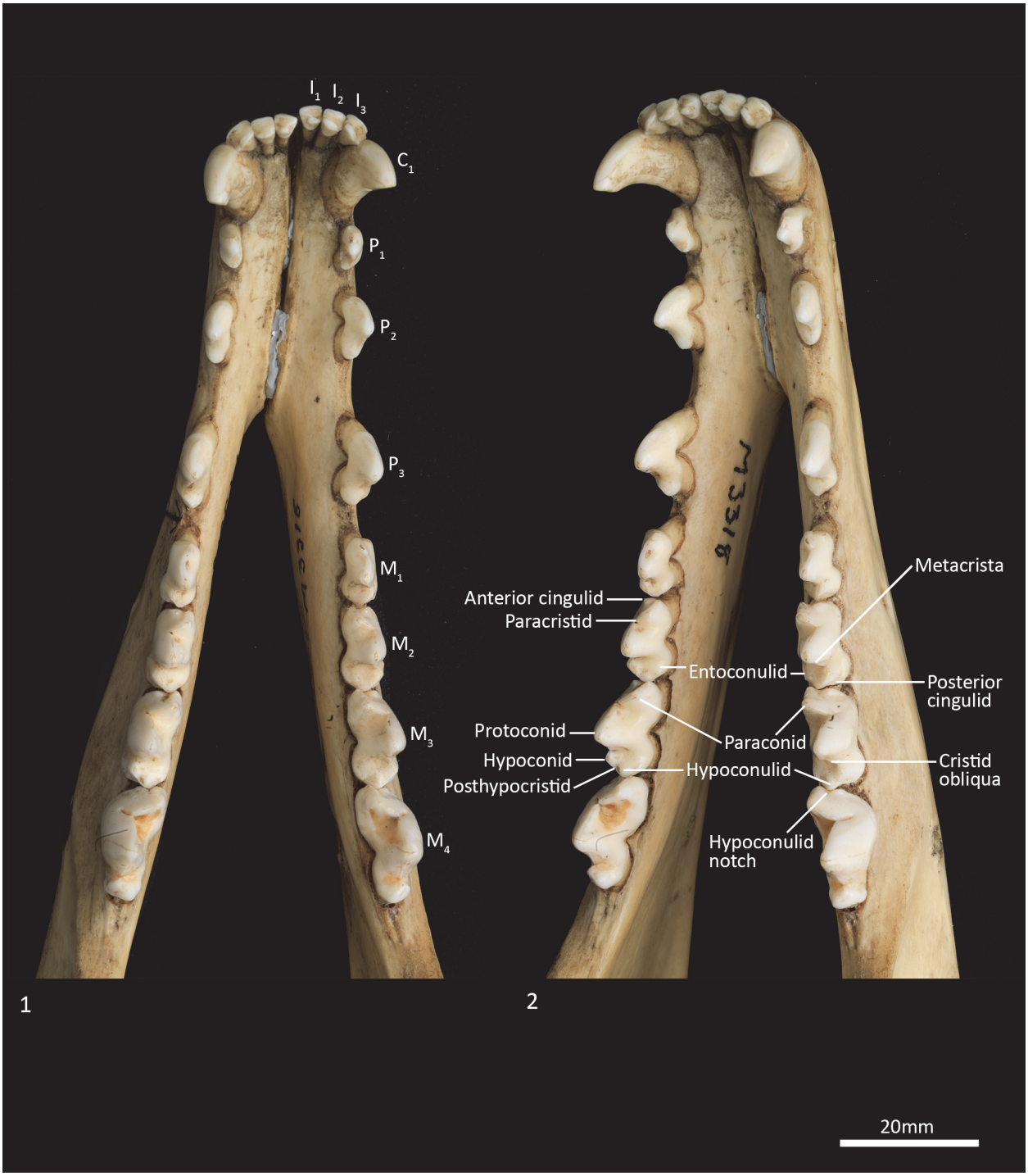

FIGURE 12. Lower dentition of WAM M195 (M3318). **1,** dorsal view; **2,** dorsolateral view. Scale bar equals 20 mm. C_1, lower canine; I_{1-3}, lower incisor 1 to 3; M_{1-4}, lower molar 1 to 4; P_{1-3}, lower premolar 1 to 3.

in size and is bladed, joining to the metastyle posteriorly; a preprotocrista is present and descends the protocone anterolingually; a postprotocrista is present and descends the protocone posterobuccally, ending at the base of the lingual flank of the metacone; dental wear also occurs along the preparacrista and postprotocrista.

M^3 is similar in morphology to M^2 except as follows: the tooth is larger in all dimensions; stylar cusp B, stylar cusp E and the protoconule are

FIGURE 13. Mandible of WAM M17189. **1,** left lateral view; **2,** right lateral view; **3,** right medial view; **4,** left medial view; **5,** occlusal view. Scale bar equals 20 mm.

absent; and the preprotocrista and postprotocrista are also absent.

M^4 differs from M^3 as follows: the tooth is smaller in all dimensions; the parastylar shelf is enlarged, with the paracone being the dominant cusp on the crown; the preparacrista is longer and straight, passing through a large ovoid stylar cusp B and terminating with a small stylar cusp A; no anterior cingulum is present; the metastylar shelf is heavily reduced, with the metacone reduced to a small cusp; and the protocone is reduced.

Lower dentition (Figures 12-13). The morphology of the $I_{1–3}$ are similar, only differing in overall size, with I_1 being the smallest tooth and I_3 being the largest. They are unirooted with an anterior cuspid and a posterior cuspid. Each cuspid has a medial crest and a lateral crest descending the crown. Between the two cuspids, there is no enamel, exposing a line of dentine. As the teeth wear, the cuspids are worn flat, resulting in a single anterior crest and a single posterior crest on the crown.

The C_1 is similar in morphology to the C^1, but it is smaller. There is a dental wear facet on the anterior surface, probably caused by tooth-on-tooth wear with the I^4, and there is a posterior wear facet near the tip of the tooth, cause by tooth-on-tooth wear with the C^1.

The $P_{1–3}$ are similar in morphology to $P^{1–3}$ and only differ in size, being larger (longer and taller but similar in width) that the $P^{1–3}$.

The M_1 is roughly rectangular in occlusal view and double rooted. There is a minute notch (hypoconulid notch) at the anterior of the tooth. There is no anterior cingulid. The trigonid is made of the very large protoconid and the much smaller paraconid. No metaconid is present. The protoconid and paraconid are connected by the paracristid, with a distinct carnassial notch just posterior to the paraconid. The metacristid descends the protocone posterobuccally and meets the very short cristid obliqua, which then rises to the tip of the hypoconid. The posthypocristid is oblique and ends at the hypoconulid. No entoconid is present. A posterior cingulid is present at the posterior end of the crown, buccal to the posthypocristid. Dental wear occurs on the tips of the paraconid, protoconid, hypoconid and along the paracristid and posthypocristid.

The M_2 is similar in morphology to the M_1 except as follows: the tooth is larger in all dimensions; an anterior cingulid is present just buccal to the anterior notch; a minute entoconid is present lingual to the hypoconid. The M_3 is similar in morphology to the M_2 except as follows: the tooth is larger in all dimensions; the carnassial notch is deeper. The M_4 is similar in morphology to the M_3 except as follows: the tooth is larger in all dimensions; the carnassial notch is deeper; the talonid is heavily reduced in size; the entoconid is absent.

Axial Skeleton

Cervical vertebrae (Figures 1, 14). The atlas has large, terminally expanded transverse processes, deep cranial articular facets and small dorsal tubercle. The ventral arch of the atlas is unfused as the lateral bodies of broad neuropophyses are widely separated. The caudal articular facets are very slightly concave, with oblique (roughly 45º) orientation to the transverse plane. The axis has a very long and deep spinous process that extends both cranially and caudally from a comparably short (craniocaudal axis) neural arch. The caudal extremity of the spinous process is extended as a long caudodorsal projection. The centrum is elongate, constricted in the mid-region and expanded both cranially and caudally for articular facets. The caudal part of the body extends caudoventrally resulting in a slightly oblique orientation of the caudal extremity. The dens (odontoid process) of the axis is robust and only moderately long. The cranial articular facets are broad, and very slightly convex. The caudal articular facet is small, ovoid, oblique in orientation from the lateral view and faces ventrolaterally. The vertebral canal is very large and roughly circular. The transverse processes extend caudolaterally and are elongate.

Cervical vertebrae 3–7 are roughly square in shape from the dorsal view. For C3 the caudal articular processes (postzygapophyses) are transversely broader and blunter than the narrower and elongate cranial articular processes (prezygapophyses), but for C4–C7 the cranial and caudal articular processes are of quite similar dimensions. Spinous processes are moderately long, narrow, sharp and caudally inclined in C3–4; they are longer and more vertical/dorsally projecting in C5–7. The cervical vertebral bodies are longer than they are transversely wide. The transverse processes are complex and varied. In C3 the transverse processes are robust caudolaterally with small, narrow points cranially lying roughly in a horizontal plane to the body of the vertebra. In C4–5, the cranial extension (tuberculum ventrale) of the transverse process becomes increasingly more enlarged and cranioventrally directed. In C6 the transverse process is further augmented by a large caudoventral expansion reminiscent of the lamina ventralis in

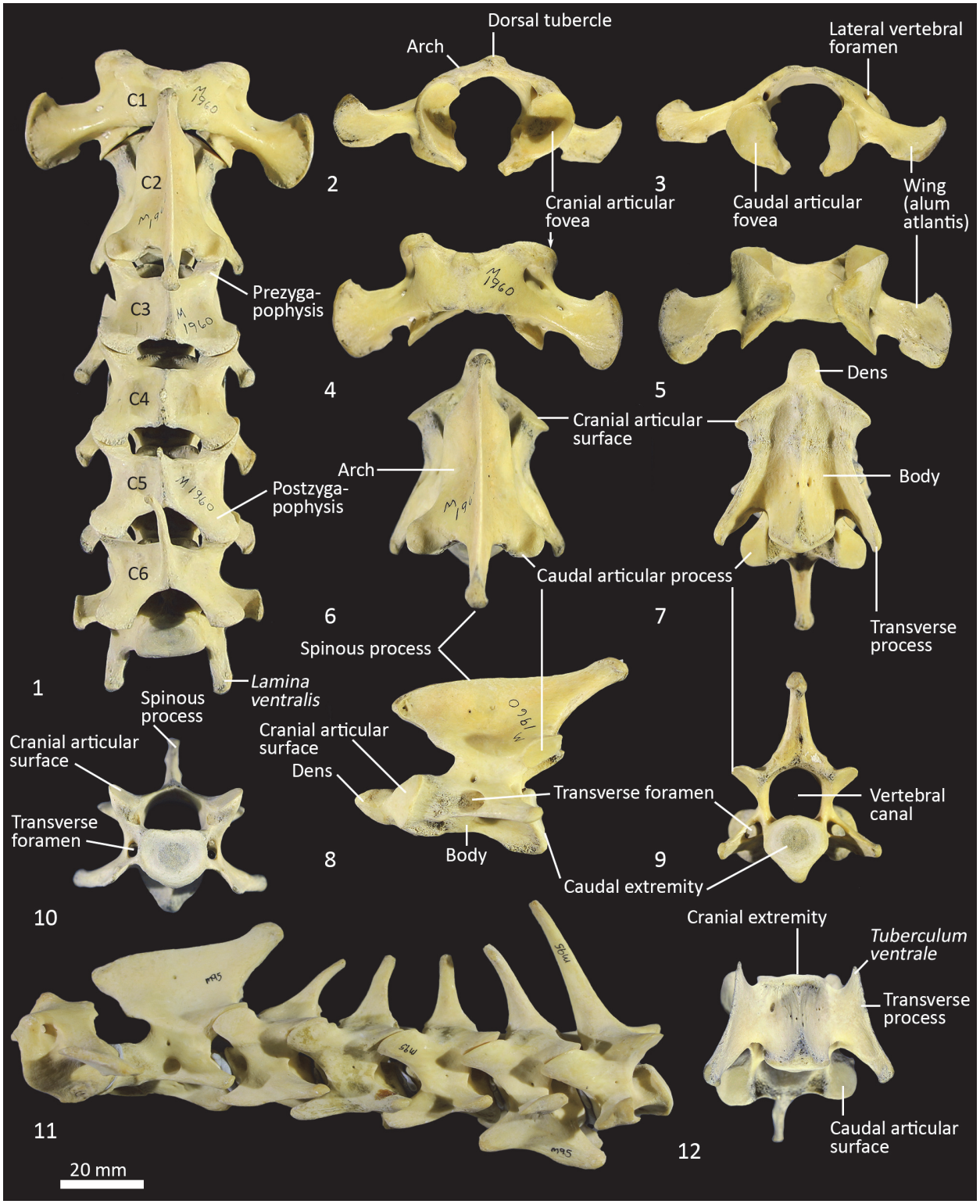

FIGURE 14. Cervical vertebrae SAMA M1960. **1,** articulated cervical vertebrae, dorsal view; **2,** atlas (C1) cranial view; **3,** atlas caudal view; **4,** atlas dorsal view; **5,** atlas ventral view; **6,** axis (C2) dorsal view; **7,** axis ventral view; **8,** axis lateral view; **9,** axis caudal view; **10,** third cervical vertebrae (C3) cranial view; **11,** articulated cervical vertebrae lateral view; **12,** C3 ventral view. Scale bar equals 20 mm.

Canis, in addition to an enlarged caudodorsal branch (tuberculum dorsale). In C7 the transverse process is relatively shorter and reduced to a blunt dorsal portion (Figure 1).

Thoracic vertebrae (Figures 1, 15). There are 13 thoracic vertebrae with very long spinous processes cranially, tending to shorter and broader spinous processes caudally. The cranial spinous processes are caudally inclined; the anticlinal vertebra is T10 and the caudal spinous processes T11–13 are very slightly cranially inclined. The thoracic centra are similar in size until T10 where they then increase in size (cross-sectional area) gradually toward the lumbar region. On the centrum of each vertebra, small demifacets mark the articulation with the heads of the ribs: the fovea costales craniales are well marked in T2-T9, then much reduced in T10-13. The transverse processes with facets for the articular part of the tubercle of the rib (diapophysis; fovea costalis processes transversi) are robust and broad; in T1 the ventral aspect of the fovea lies just above the dorsal plane of the centrum and the fovea is deeply concave. In each successive vertebra, the transverse process becomes blunter and slightly more dorsally placed from the centrum. The cranial articular processes (prezygapophyses) of T1 are broad and flat. From T2–T11 the prezygapophyses are very short and have small ovoid, dorsally facing articular facets. The prezygapophyses of T10–13 become increasingly extended with enlarged, raised and medially inclined mammillary processes rising beyond the cranial articular facets. The caudal articular processes (postzygapophyses) are small and ventrally orientated from T-10, and from T11–T14 become increasingly enlarged, dorsally situated and laterally inflected. The specimen photographed in Figure 15 (SAMA M95) was a large male and shows some pathological changes to the ventral margins of the thoracic centra, particularly in T1, T3 and T4.

Lumbar vertebrae (Figures 1, 16). There are six lumbar vertebrae with long, dorsoventrally compressed centra. They are oval in section, with marked midventral crests and large rectangular spinous processes. The pre- and post-zygapophyses are short and robust; well-developed mammillary processes (metapophyses) appear to restrict movement at the joints between the articular processes. The transverse processes from the craniodorsolateral part of the centrum (diapophysis) are relatively short and blunt on L1 and become increasingly longer from L1-6, extending laterally and then arcing cranioventrally.

Sacral vertebrae (Figure 17). The sacrum is comprised of two fused sacral vertebrae that are easily distinguished from one another by a large opening into the sacral canal dorsally and a pair of large sacral foramina laterally. From the cranial view, the base of the sacrum (cranial extremity of centrum S1) is a broad, dorsoventrally compressed oval. The prezygapophyses of S1 are short and widely spaced and the cranial articular facets are large. The wing (ala) formed from the transverse processes of S1 is robust and much broader than the transverse processes of S2, which form a long (craniocaudally) horizontal shelf on the lateral aspect. Spinous processes of S1 and S2 are very weakly developed and remain completely separate from each other. The postzygapophyses are small.

Caudal vertebrae (Figures 1, 17). There are 21–22 caudal vertebrae for the specimens we observed. Six proximal caudal vertebrae with large transverse process and distinct prezygapophyses; the width across the transverse processes is greater than centrum length and gradually diminishes from Ca1–6. Caudals 1–4 have small, ovoid articular facets and flared mammillary processes. Postzygapophyses are well developed and extend beyond the caudal extremity of the centrum in Ca1–3 and then rapidly diminish in size to Ca5 where they are present as two small spines. Neural spines are poorly-developed/virtually absent. Transitional caudal vertebra (Ca7) has two pairs of transverse processes, small cranial and larger caudal; the prezygapophyses and postzygapophyses are rudimentary and have a persistent vertebral/neural canal. The distal caudal series Ca8–22, have small cranial and caudal transverse processes, and very small prezygapophyses, diminishing along the series. The centra are remarkably consistent in length Ca7–16, though becoming more gracile along the series.

Associated with the caudal vertebrae of marsupials are the chevron bones, derived from the caudal haemal arches. As described by W.H. Flower (1876, p. 64-65); “Connected with the under-surface of the caudal vertebrae of many mammals which have the tail well developed, are certain bones, formed more or less in the form of an inverted arch, called *chevron bones*. These are always situated nearly opposite to the intervertebral space and are generally articulated both to the vertebra in front and in the vertebra behind… they are usually articulated movably to prominences *(hypapophyses)* on the lower surface of the body of the vertebra, but occasionally become ankylosed to it. They serve to give a larger surface of attach-

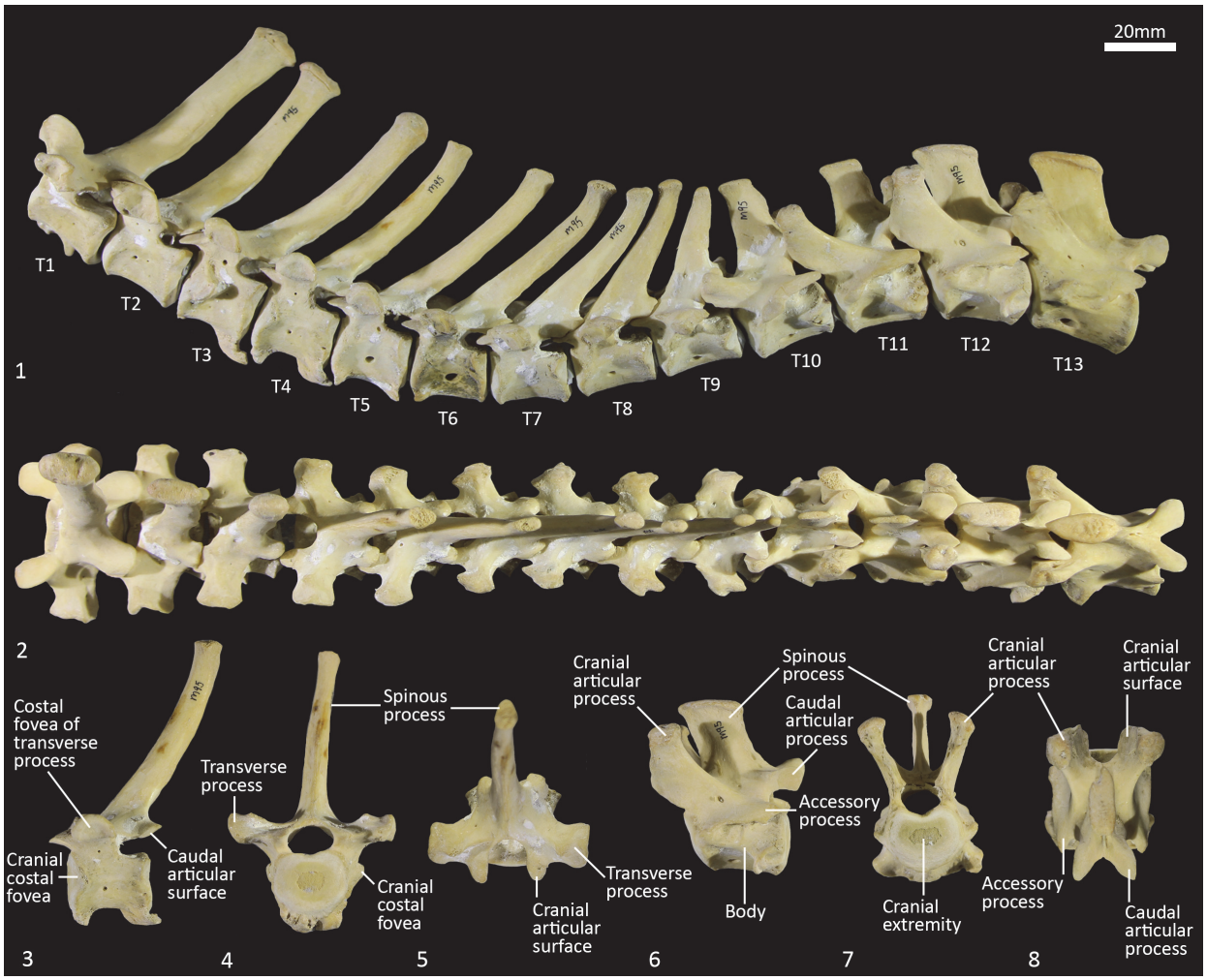

FIGURE 15. Thoracic vertebrae SAMA M95. **1,** complete thoracic series (T1-T13) lateral view; **2,** dorsal view; **3-5,** fourth thoracic vertebra lateral (**3**), cranial (**4**) and dorsal (**5**) view; **6-8,** twelfth thoracic vertebra lateral (**6**), cranial (**7**) and dorsal (**8**) view. Scale bar equals 20 mm.

ment for the inferior muscles of the tail and also to protect the caudal vessels, which run within the canal formed by the series of these bony arches…". The chevron bones of *Thylacinus* are small relative to the size of the caudal vertebrae. The most proximal chevron bone is subtriangular and deeply concave; the chevron bones of the mid-tail are keel shaped, and those toward the distal region of the tail are rectangular in outline from ventral view as illustrated by the examples in Figure 17.

Forelimb

Scapula (Figures 18-20). The overall outline is sub-rectangular; the supraspinous and infraspinous fossae are roughly equal in size. The supraspinous fossa is sub-triangular, with its apex at the rounded cranial angle and with a flared cranial border. The infraspinous fossa is elongate in the dorsoventral axis; the caudal angle is roughly 100º, resulting in a triangular shape. The scapular notch is very shallow, and the neck of the scapula is very broad. The scapular spine is long, extending to the cranial angle; the crest of the spine is high and curves caudally over the infraspinous fossa. The acromion is moderately long and broad, but not especially robust; it does not extend distally beyond the level of the supraglenoid tubercle. The glenoid fossa is fairly circular in shape and shallow. The supraglenoid tubercle is low and flat; the coracoid process is distinct from supraglenoid tubercle and extends medially over a deep notch. The subscapular fossa is gently undulating and depressed toward the caudal border; the facies serrata is

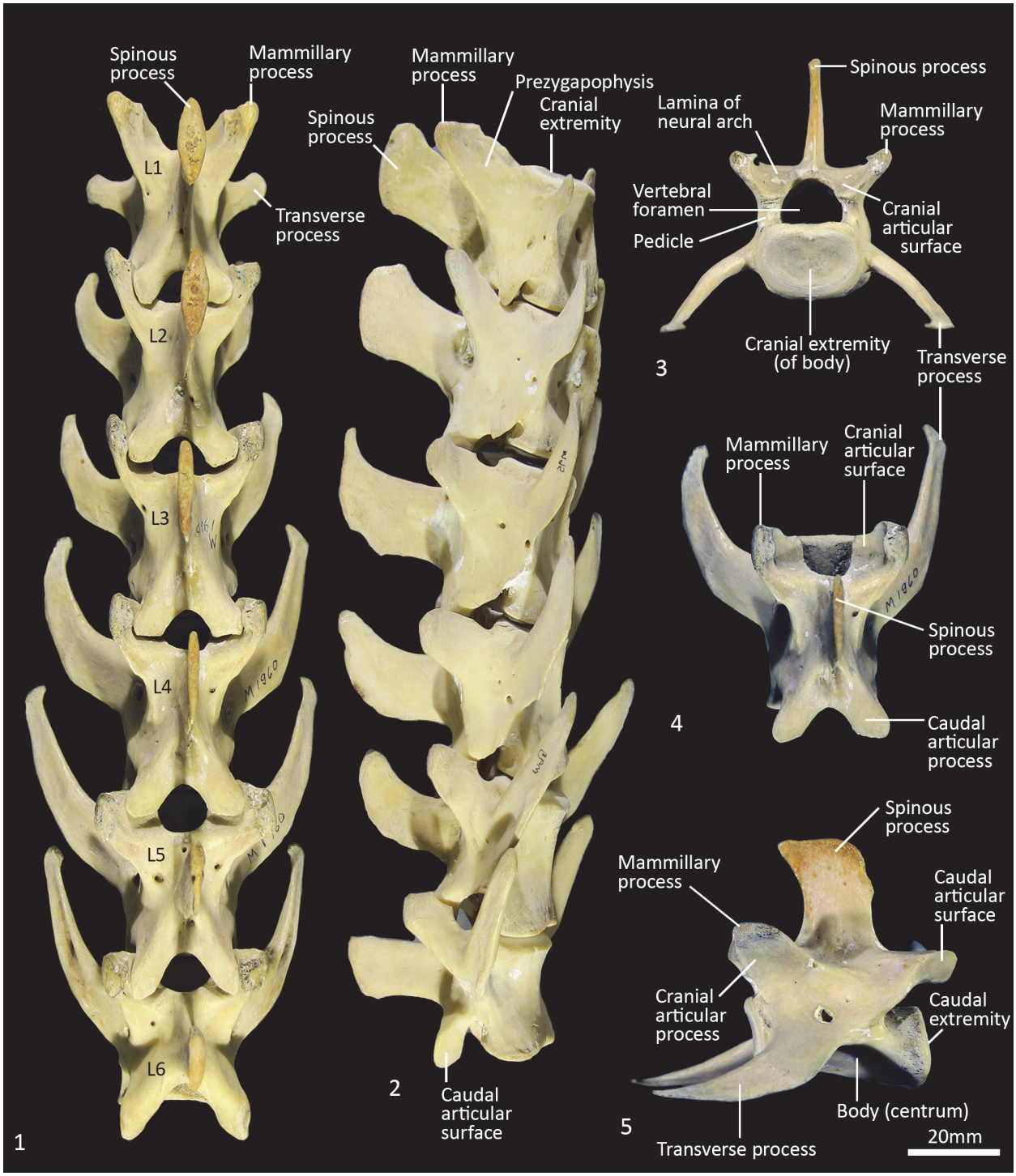

FIGURE 16. Lumbar vertebrae SAMA M1960. **1,** complete lumbar series (L1-L6), dorsal view; **2,** lateral view; **3,** third lumbar vertebra (L3) cranial view; **4,** L3 dorsal view; **5,** L3 lateral view. Scale bar equals 20 mm.

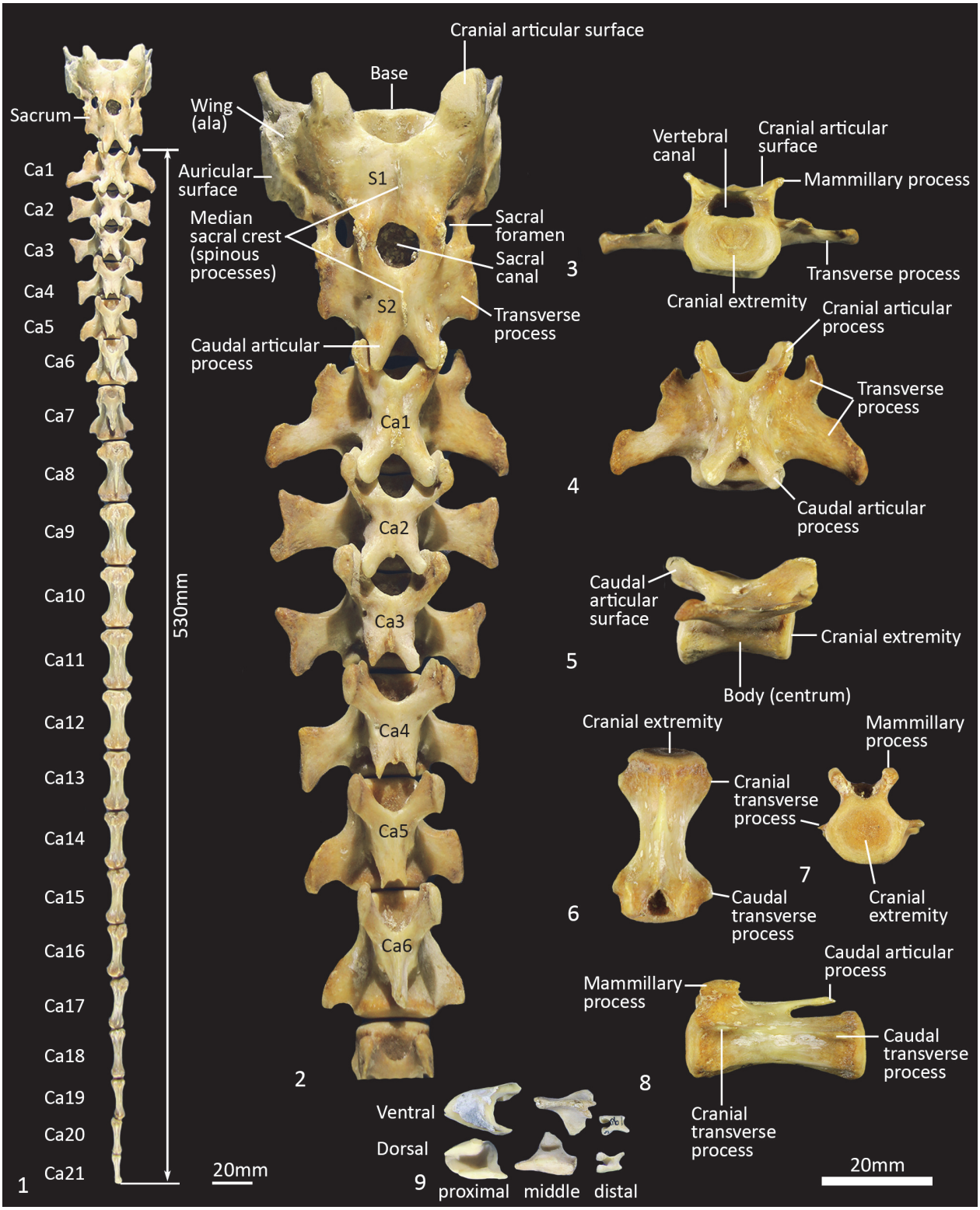

FIGURE 17. Sacral and caudal vertebrae SAMA M1960. **1,** complete sacro-caudal series, dorsal view; **2,** sacrum and proximal caudal series, dorsal view; **3,** first caudal vertebra (Ca1) cranial view; **4,** Ca1 dorsal view; **5,** Ca1 lateral view; **6,** eighth caudal vertebra (Ca8) ventral view; **7,** Ca8 cranial view; **8,** Ca8 lateral view; **9,** examples of proximal, middle and distal chevron bones from ventral and dorsal views. Scale bar equals 20 mm.

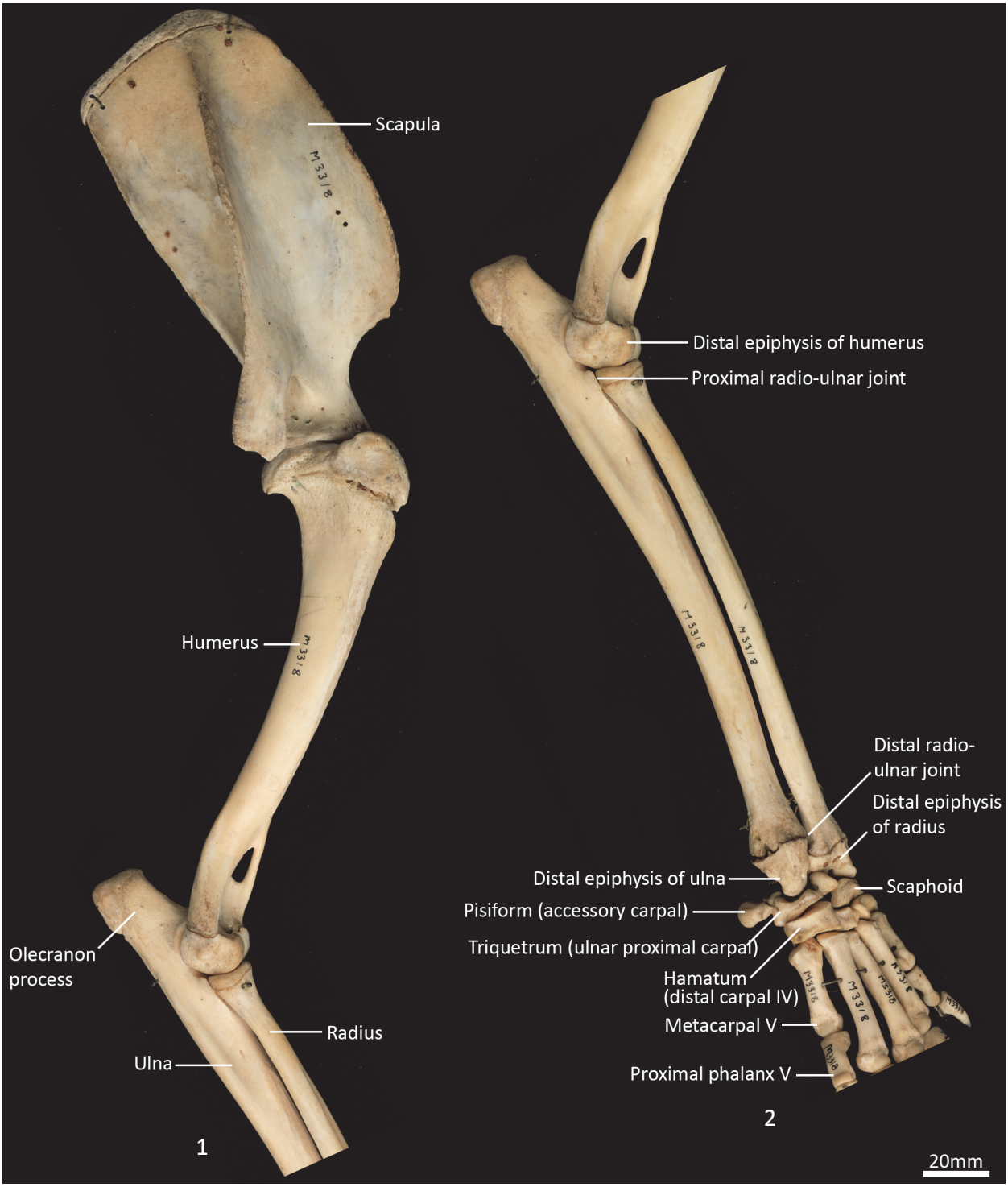

FIGURE 18. Forelimb (right) topography WAM M195 (M3318). **1,** Proximal; **2,** distal elements. Scale bar equals 20 mm.

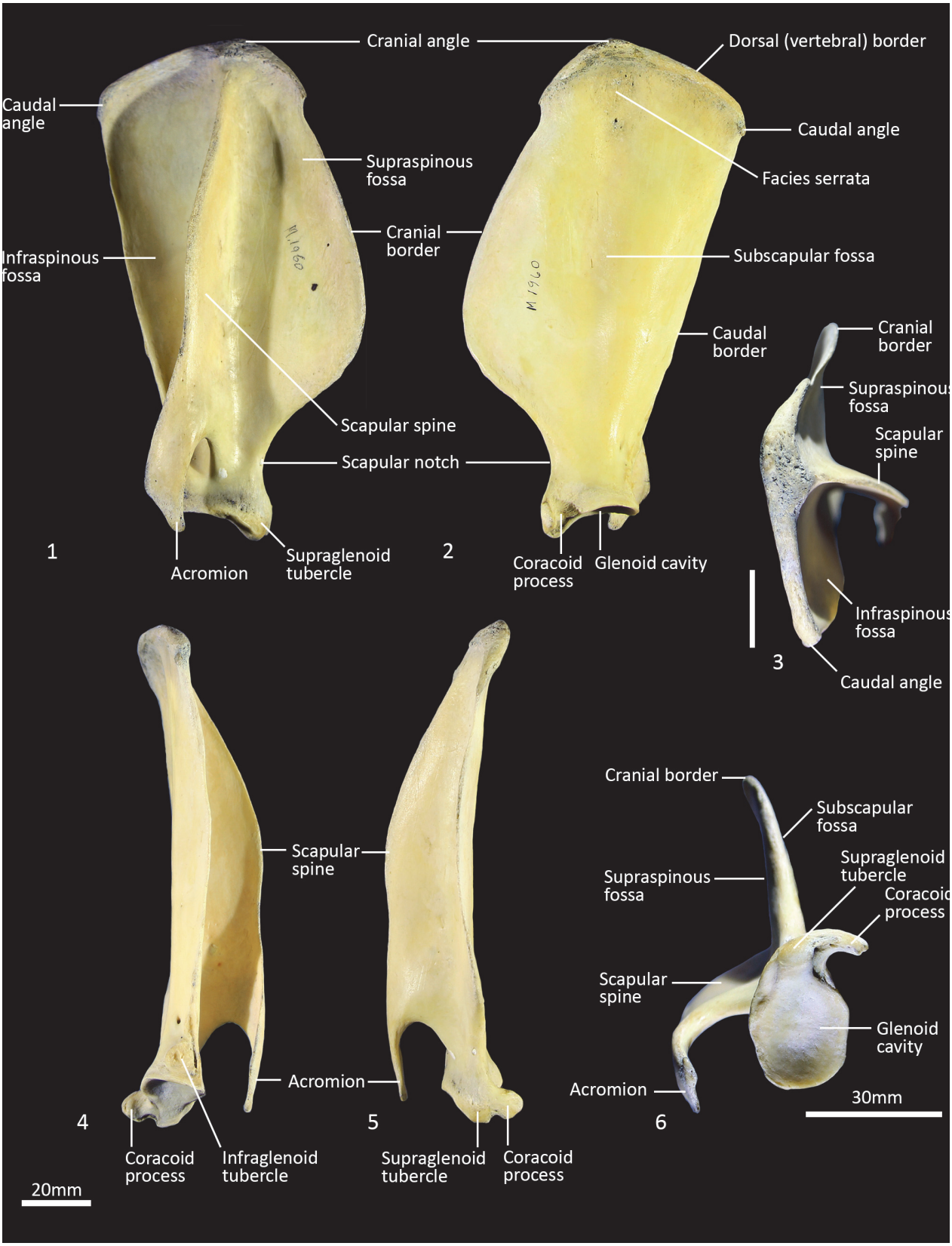

FIGURE 19. Scapula (right) SAMA M1960. **1,** lateral view; **2,** medial view; **3,** dorsal view; **4,** caudal view; **5,** cranial view; **6,** glenoid view. Scale bar equals 20 mm; NB **5** and **6** not to scale.

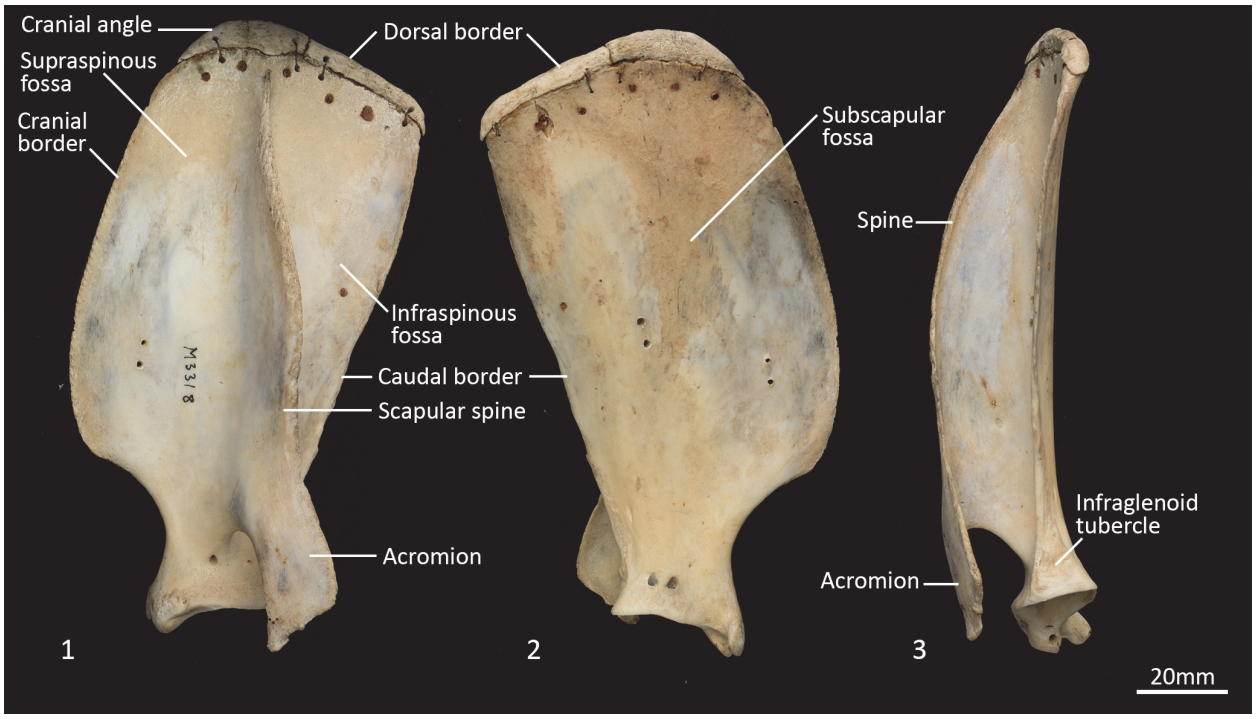

FIGURE 20. Scapula (left) WAM M195 (M3318). **1,** lateral view; **2**, medial view; **3,** caudal view. Scale bar equals 20 mm.

observable in the region adjacent to the cranial angle. The juvenile scapula is relatively shorter in proximodistal axis, resulting in a more square shape and shorter acromion.

Clavicle (Figure 21). The clavicle is much reduced, fairly thin and flat. The body curves ventrally toward the very slightly expanded acromial extremity. The sternal end tapers.

Humerus (Figures 22-23). The humerus is long and straight in cranial view, and the transverse diameter of the diaphysis is relatively similar throughout. From the medial view the shaft is very slightly sinuous; the craniocaudal diameter is greater proximally than distally. The articular surface of the head is caudally placed and circular from proximal view. The neck is pronounced. The greater tubercle is very broad, cranially displaced and extends above the articular surface of the head. The lesser tubercle is medially placed and much smaller than the greater tubercle. The intertubercular (bicipital) groove is pronounced, deeply concave and moderately narrow. The pectoral crest is not strongly pronounced, and extends from the greater tubercle to a very small deltoid tuberosity approximately two-fifths along the length of the shaft. A small teres tubercle sits adjacent to the sulcus for the insertion of m. latissimus dorsi, on the medial aspect of the shaft, approximately one-quarter of the length from the proximal extremity. The distal extremity is narrow, flaring only slightly to the medial and lateral epicondyles. The lateral extensor ridge is present, but slight; and a process for attachment of the m. brachioradialis is absent. The medial epicondylar ridge is quite thin and cranially placed over a large supracondylar (entepicondylar) foramen. The olecranon fossa is large and deep. The articular surface of the trochlea is narrow, deeply saddle-shaped and constricted medially; the capitulum is narrow and sub-rounded.

Ulna (Figures 18, 24-25). The ulnar shaft is long and very slightly curved; the proximal half curves slightly laterally and the distal half slightly caudally (the latter being the opposite of that seen in macropodids and arboreal marsupials). The proximal shaft is slightly mediolaterally compressed; the distal half is only slightly tapered. The olecranon is moderately long and quite deep. The trochlear notch is deep. The proximal margin with anconeal process is pronounced, broad and high, projecting cranially. The distal margin of the trochlear notch has a high coronoid process that extends cranially; medially the proximal and distal margins of the trochlear notch flare to accommodate the hourglass shape of the humeral trochlea. The proximal radial fossa is deeply concave and flared laterally. The ulnar tuberosity is a small rugosity marking the

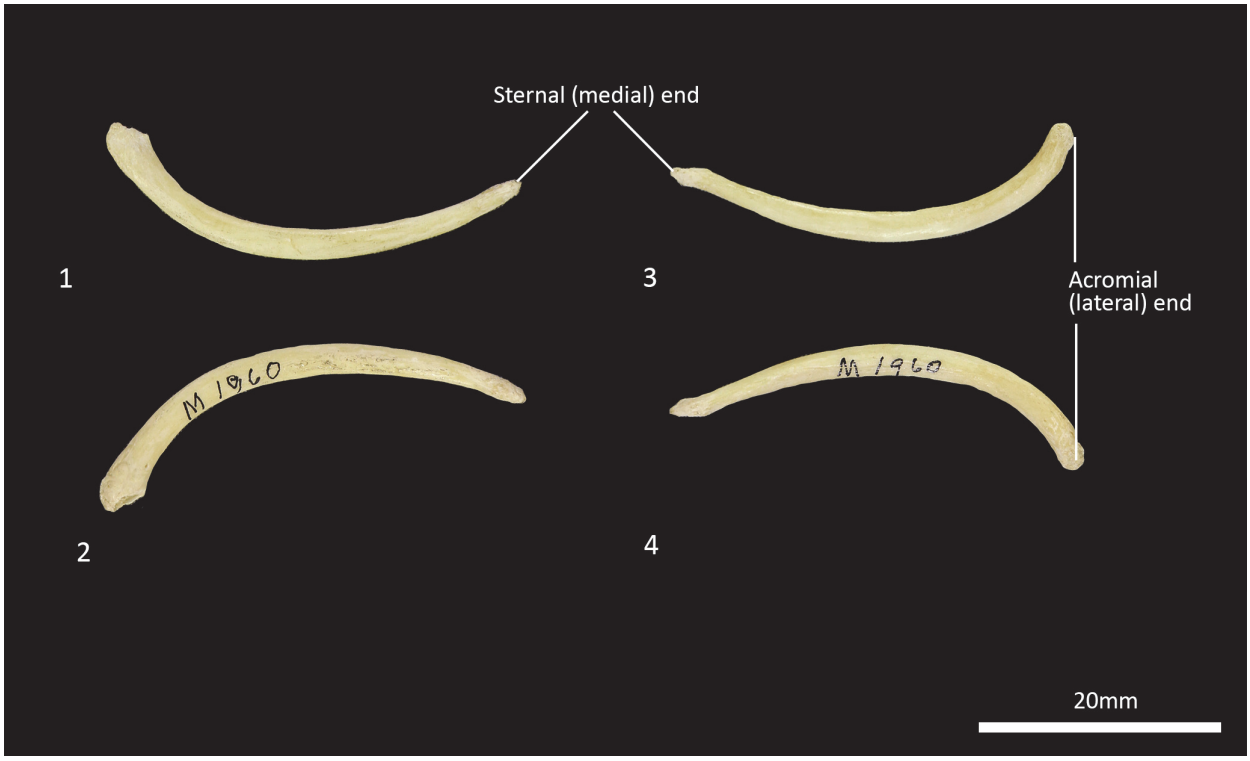

FIGURE 21. Clavicles SAMA M1960. **1,** left lateral view; **2,** left medial view; **3,** right lateral view; **4,** right medial view. Scale bar equals 20 mm.

ular facet. The articular surface for the carpal bones (scaphoid and lunatum) is roughly rectangular in shape and has an undulating surface that extends smoothly onto the blunt radial styloid process.

Carpus (Figures 26-27). Eight distinct carpal bones are present within the thylacine carpus, which on the whole, appear relatively short in their longitudinal axis but transversely broad. The scaphoid is proximo-distally compressed with undulating articular surfaces proximally for the radius and distally for the trapezoid and capitulum. The caudomedial process (for attachment of the flexor retinaculum) is poorly developed. The lunatum has a rounded, convex proximal surface for the articulation with the distal radius. The triquetrum is broad with a large, concave articular surface to receive the ulnar styloid process. The pisiform(e) is broad, with a wide articular surface for the triquetrum and a large, bulbous free end for the insertion of the m. flexor carpi ulnaris. The distal row comprises a small trapezium, trapezoid and capitatum and a broad, proximodistally compressed hamatum. The hamulus (hook of the hamate for attachment of the flexor retinaculum) is relatively slightly developed. The hamatum articulates with MCV and half of MCIV, the capitatum corresponding metacarpal; proximal phalanges I and V are relatively longer. From the lateral view, the proximal phalanges are proximally enlarged around the articular surface for the attachment of collateral ligaments. In each, the shaft is dorsoventrally compressed and dorsally arched. The distal end becomes more robust, supporting a broad convex trochlea with small circular fossae on either side for the origin of the collateral ligaments. The middle phalanges II to IV are roughly half the length of their corresponding proximal phalanx. They are dorsoventrally compressed, with transversely broad articular surfaces proximally and distally. The distal (ungual) phalanges are slightly longer than the corresponding medial phalanx and support strong, moderately curved ungual processes and large, flat flexor tubercles. They display a distinct proximal collar that supports/ braces the unguis (keratin sheath of the claw).

Hindlimb

Pelvis (Figures 29-30). The body of the ilium is robust as it extends cranially from the acetabulum before becoming flattened into the wing of the ilium. From the ventral view, the iliac wing arches laterally toward its cranial margin, the iliac crest; the cranial ventral iliac spine (cranioventral apex of

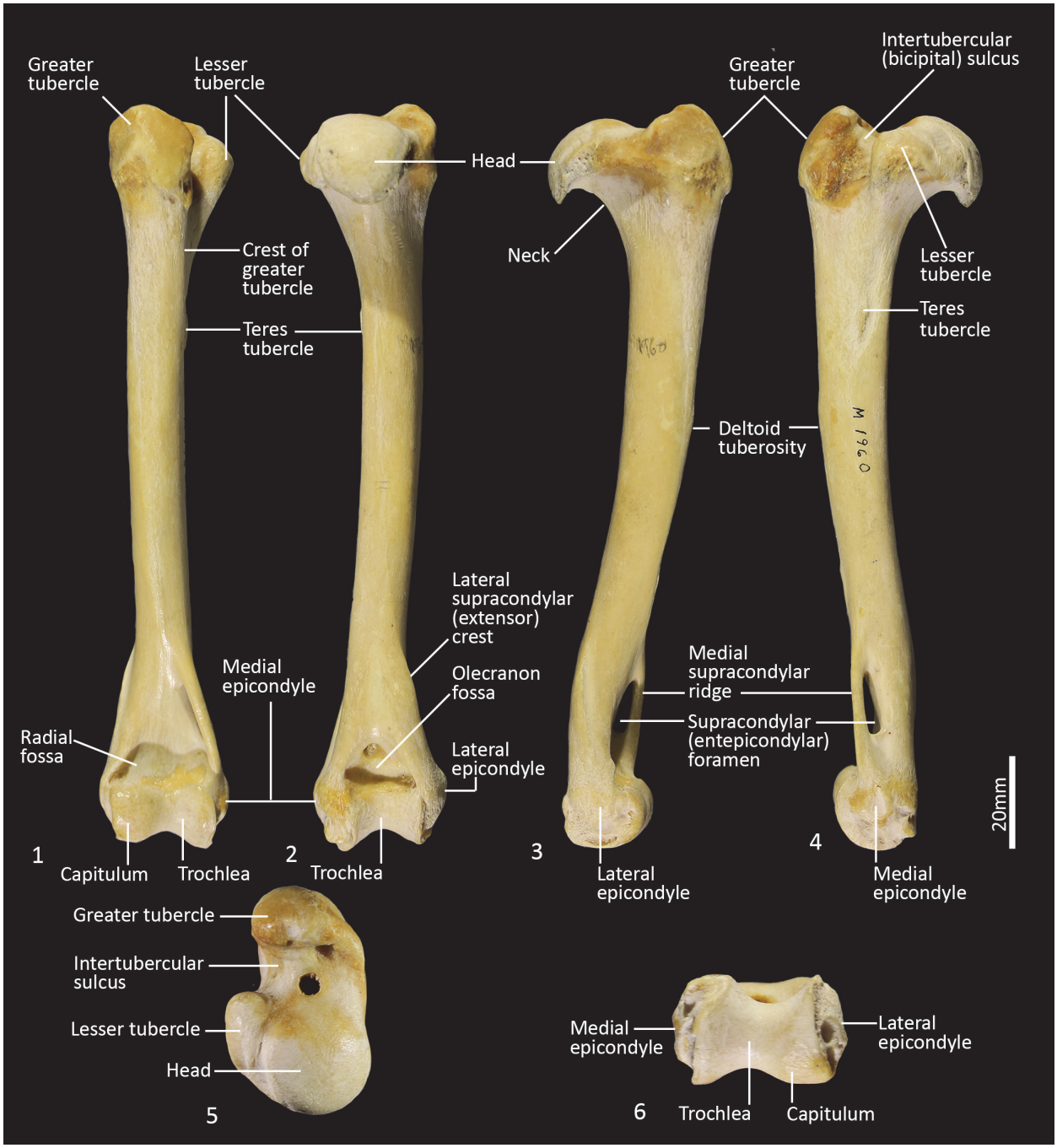

FIGURE 22. Right Humerus SAMA M1960. **1,** cranial view; **2,** caudal view; **3,** lateral view; **4,** medial view; **5,** proximal view; **6,** distal view. Scale bar equals 20 mm; NB **5** and **6** not to scale.

the iliac wing) lies just outside the lateral margin of the ischiatic tuberosity, giving the pelvis a fairly rectangular shape in the dorsoventral plane. The dorsal margin of the iliac wing flares caudally from the dorsal margin of the iliac crest (craniodorsal iliac spine) to the caudodorsal iliac spine. Immediately cranial to the acetabulum, the rectus tubercle is broad and rugose. The iliac fossa is rectangular in shape and very shallow; the gluteal fossa is more irregular in contour, but also not deep. The lunate articular surface in the acetabulum is interrupted by a wide acetabular notch separating the iliocotylar tuberosity from the larger ischiocotylar portion. There is a small, cranially projecting iliopubic (iliopectineal) eminence at the junction of the ilium and pubis on the rim of the pelvic inlet. The

FIGURE 23. Humerus (left) WAM M195 (M3318). **1,** cranial view; **2,** caudal view; **3,** lateral view; **4,** medial view; **5,** proximal view; **6,** distal view. Scale bar equals 20 mm; NB **5** and **6** not to scale.

ilio-ischiatic junction and dorsolateral aspect of the ischiatic ramus are marked by a series of slightly raised ischiatic spines. The ischiatic table is long, broad and shallowly concave. The ischiatic tuberosity is large and rounded. The obturator foramen is long and ovoid. From the caudal view, the angle made between the two ischia is obtuse. The pelvic (pubic+ischiatic) symphysis is very long. The morphology of the pubic tubercle is variable between specimens ranging from a single, moderately large and projecting tubercle, to a pair of low, broad peaks on either side of the midline. This region is the site of attachment of the very short and reduced epipubic bones in thylacines.

Epipubic bones (Figure 30). Generally, marsupials have a pair of elongated, flattened and slightly

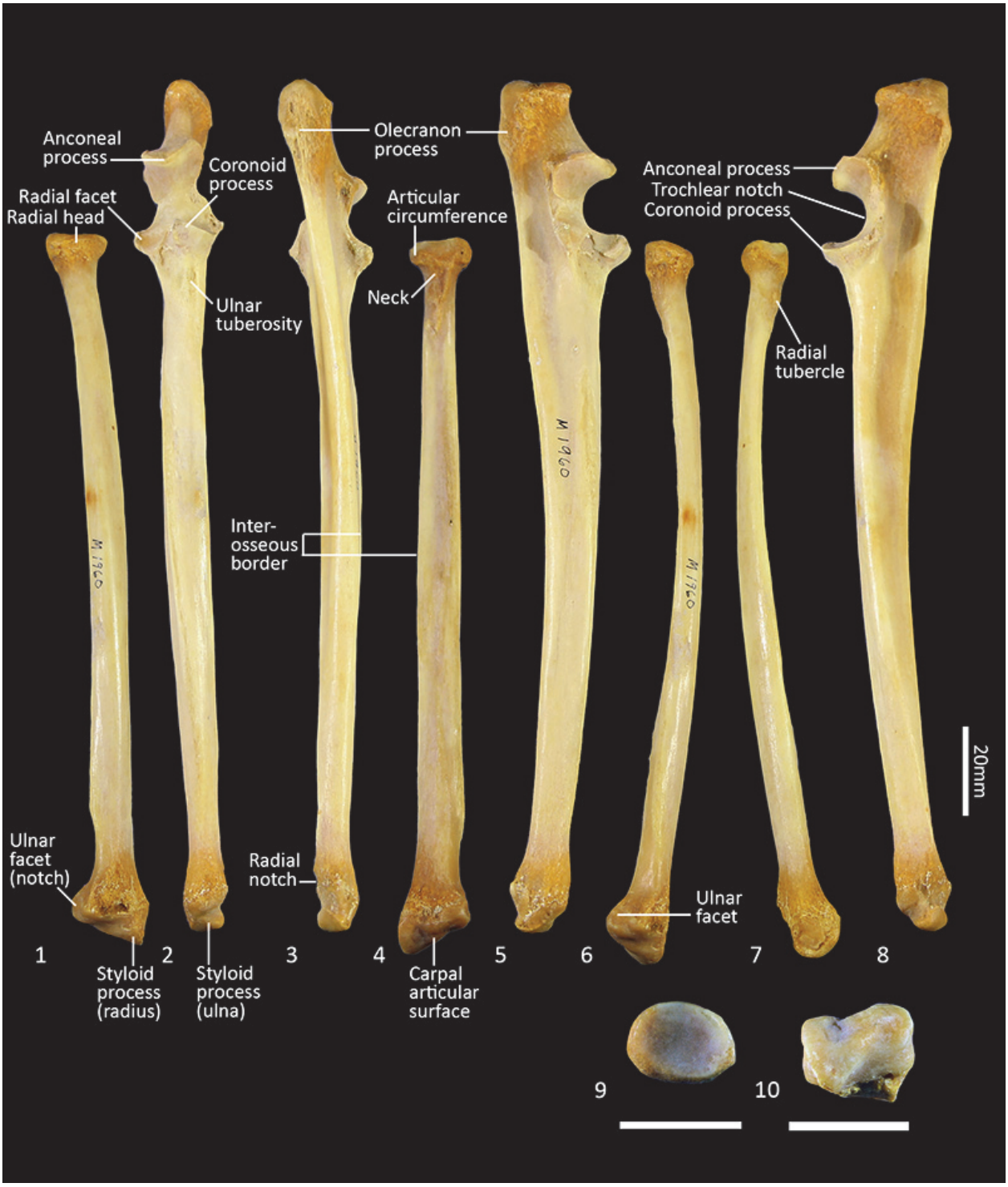

FIGURE 24. Ulna and radius (right) SAMA M1960. **1,** radius cranial view; **2,** ulna cranial view; **3,** ulna caudal view; **4,** radius caudal view; **5,** ulna lateral view; **6,** radius lateral view; **7,** radius medial view; **8,** ulna medial view; **9,** radius proximal view; **10,** radius distal view. Scale bar equals 20 mm; NB **9** and **10** not to scale.

FIGURE 25. Ulna and radius (left) WAM M195 (M3318). **1,** ulna cranial view; **2,** ulna medial view; **3,** ulna lateral view; **4,** radius lateral view; **5,** radius cranial view; **6,** radius medial view; **7,** radius proximal view; **8,** radius distal view. Scale bar equals 20 mm; NB **7** and **8** not to scale.

FIGURE 26. Manus (left) SAMA M1960. **1,** proximal view (digitigrade posture); **2,** lateral view (digitigrade posture); **3,** dorsal view (plantigrade posture); **4,** palmar/ventral view (plantigrade posture); **5,** medial view (digitigrade posture). Scale bar equals 20 mm.

FIGURE 27. Carpal bones (left) SAMA M1960, dorsal, ventral, proximal, distal, medial and lateral views. **1-6,** Scaphoid; **7-12**, lunatum; **13-18**, triquetrum; **19-24,** pisiforme; **25-30**, trapezium; **31-36**, trapezoid; **37-42**, capitatum; **43-48**, hamatum. Scale bar equals 10 mm.

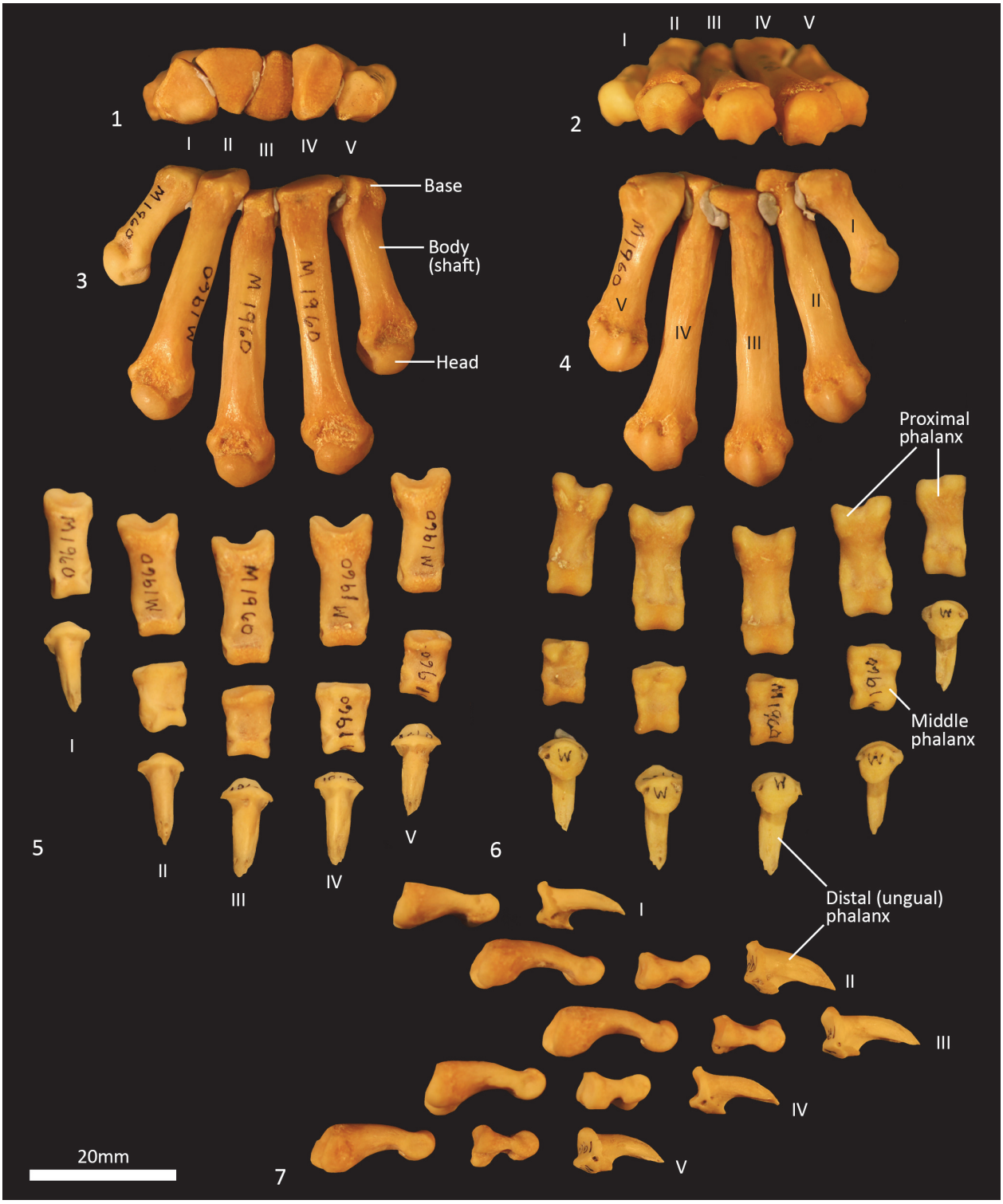

FIGURE 28. Metacarpals and phalanges (left) SAMA M1960. **1-4,** Metacarpals proximal view (**1**); distal view (**2**); dorsal view (**3**); ventral (palmar) view (**4**); **5-7,** phalanges dorsal view (**5**); ventral (palmar) view (**6**); lateral view (**7**). Scale bar equals 20 mm.

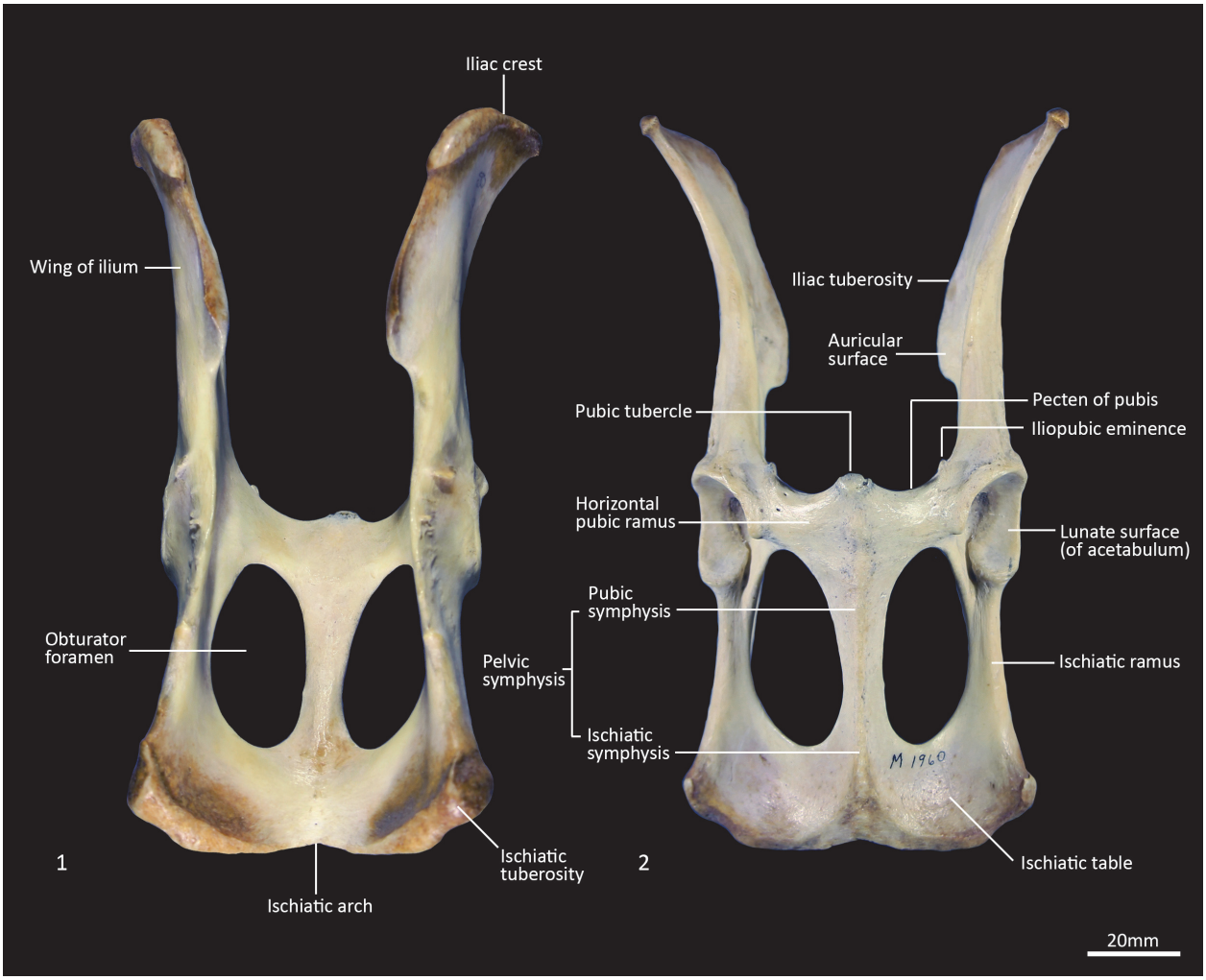

FIGURE 29. Pelvis SAMA M1960 (landscape). **1,** ventral view; **2,** dorsal view. Scale bar equals 20 mm.

curved epipubic bones that articulate with the anterior edge of the pubis, near the symphysis, which extend craniolaterally within the layers of the abdominal muscles. As reported by Flower (1876, p. 296), "Though largely developed in the Dasyures, in the allied genus *Thylacinus,* they are represented only by small, unossified fibrocartilages." Associated with were a pair of very short epipubic bones, associated with specimen M665. They are approximately 1 cm long, dorsoventrally flattened and roughly oval in shape. They are composed of spongy bone with surrounding cartilage, particularly at their base.

Femur (Figures 31-33). The femur is elongate and gracile. The head is relatively large, hemispherical and protrudes medially and slightly cranially; the neck is proximomedially directed and moderately long. The proximal cranial surface, between the head and the lateral trochanteric crest is short and broad. The greater trochanter is relatively small; from the cranial view the apex is narrow and does not extend dorsally beyond the height of the femoral head. The lesser trochanter is pronounced; the pointed apex is connected to the proximal femoral shaft by a narrow, oblique crest. The intertrochanteric line has a pronounced crest adjacent to the femoral head. The trochanteric fossa is broad and forms a deep pocket that is restricted to the middle portion of the greater trochanteric crest. From the cranial view, the shaft is very slightly narrower proximally than distally, and slightly medially bowed in the distal two-thirds. From the lateral view, the shaft bows slightly cranially. The linea aspera extends almost the full length of the caudal aspect of the shaft. The distal epiphysis is short and broad from cranial view; the condyles are short in caudal view and deep from distal view. The condyles are sub-equal in size and of equal depth

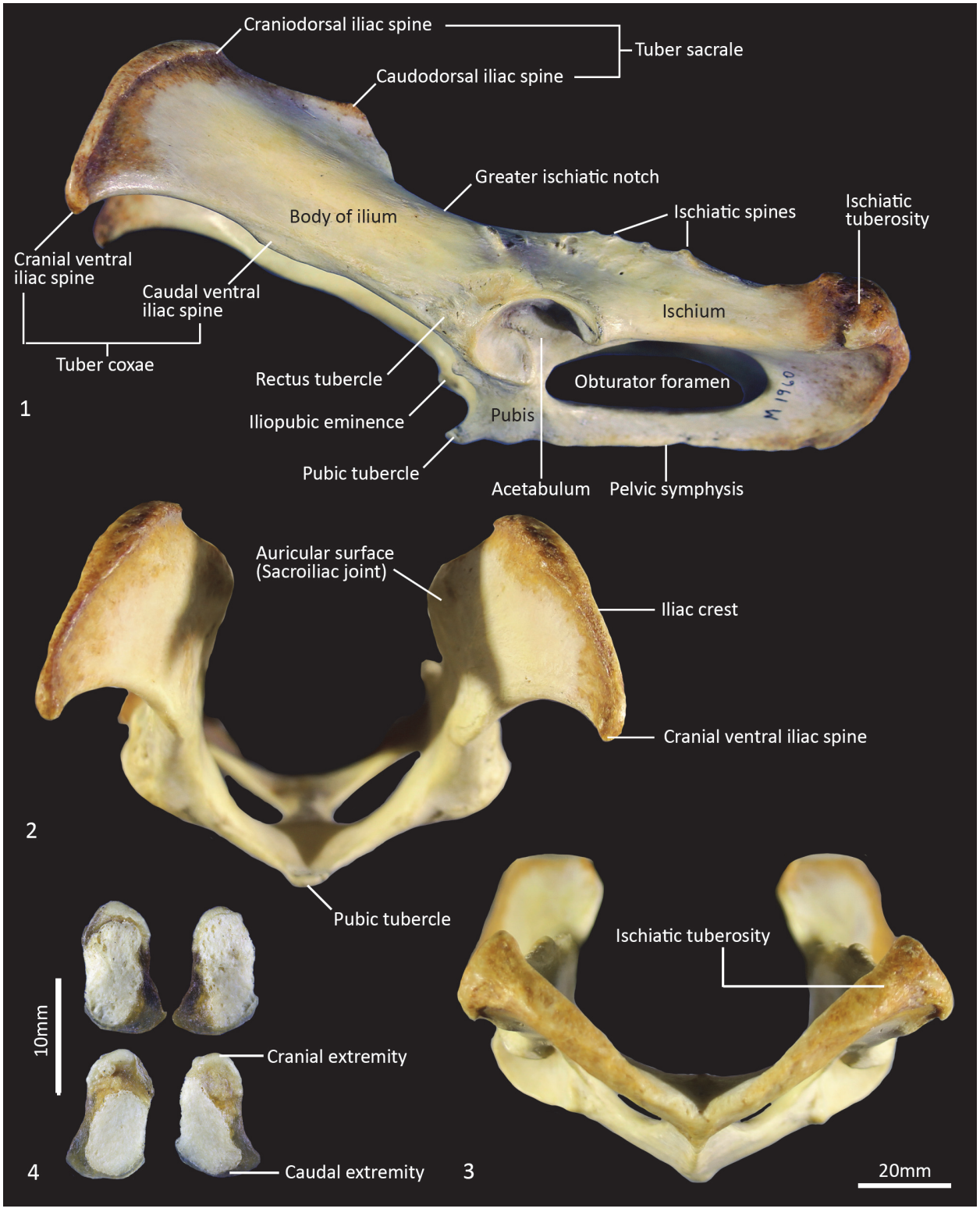

FIGURE 30. Pelvis SAMA M1960. **1,** left lateral view; **2,** cranial view; **3,** caudal view. Scale bar equals 20 mm. **4,** Epipubic bones. Scale bar equals 10 mm.

FIGURE 31. Pelvis WAM M195 (M3318) (landscape). **1,** dorsal view; **2,** ventral view; **3,** right lateral view. Note missing epiphyses and unfused pelvic symphysis. Scale bar equals 20 mm.

craniocaudally; the medial condyle projects slightly further distally. The trochlear crests are low, smoothly rounded and flare away from the midline. The intercondylar fossa is deep, with oblique orientation when viewed distally resulting from the medially aligned condyles. The medial and lateral epicondyles are pronounced and extend abaxially beyond the margins of the condyles. As with most marsupials, the patella is absent in thylacines and is instead represented by a tendinous pad.

Tibia (Figures 34-36). The tibia is elongate and approximates the femur in length. The tibial plateau is subtriangular from proximal view, deeper in craniocaudal axis than transversely wide. The condyles are relatively small, semicircular in shape and flat in profile. A distinct muscular groove for the m. tibialis cranialis? separates cranial tibial tuberosity from the lateral condyle. The tibial tuberosity is blunt and rounded. The cranial tibial crest is low and rounded with no distinct augmentation of the cranial border from the lateral view. The proximal fibular facet is small, ovoid and caudolaterally orientated. The popliteal surface is smoothly concave. The tibial diaphysis is transversely narrow throughout relative to the craniocaudal depth; this is most obvious in the proximal shaft, where the craniocaudal depth is almost twice the transverse dimension. The distal diaphysis is more ovoid in transverse section, rather than subtriangular, and bowed slightly laterally. The distal epiphysis is distinctive with a very short and blunt medial malleolus and very shallow articular surface for the talus. From the distal view, the articular area is roughly square in outline with an axial depression for the low medial crest of the talus. On the anterior surface the epiphysis has a broad, rugose tubercle and proximal to this a broad, shallow sulcus on the lateral aspect of the distal shaft for the *m. popliteus*?.

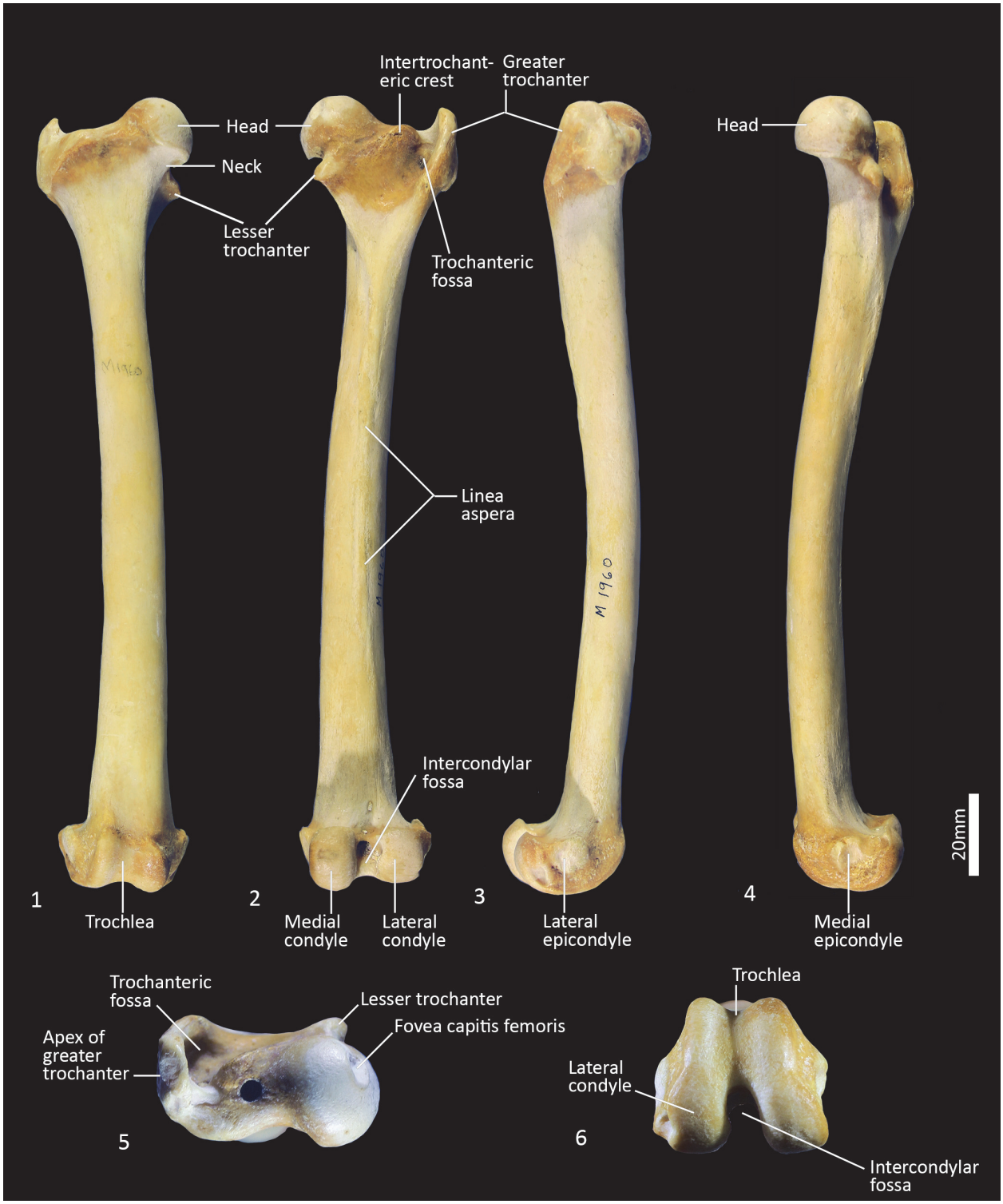

FIGURE 32. Femur SAMA M1960. **1,** cranial view; **2,** caudal view; **3,** lateral view; **4,** medial view; **5,** proximal view; **6,** distal view. Scale bar equals 20 mm.

FIGURE 33. Femur WAM M195 (M3318). **1,** cranial view; **2,** caudal view; **3,** lateral view; **4,** medial view; **5,** proximal view; **6,** distal view. Scale bar equals 20 mm.

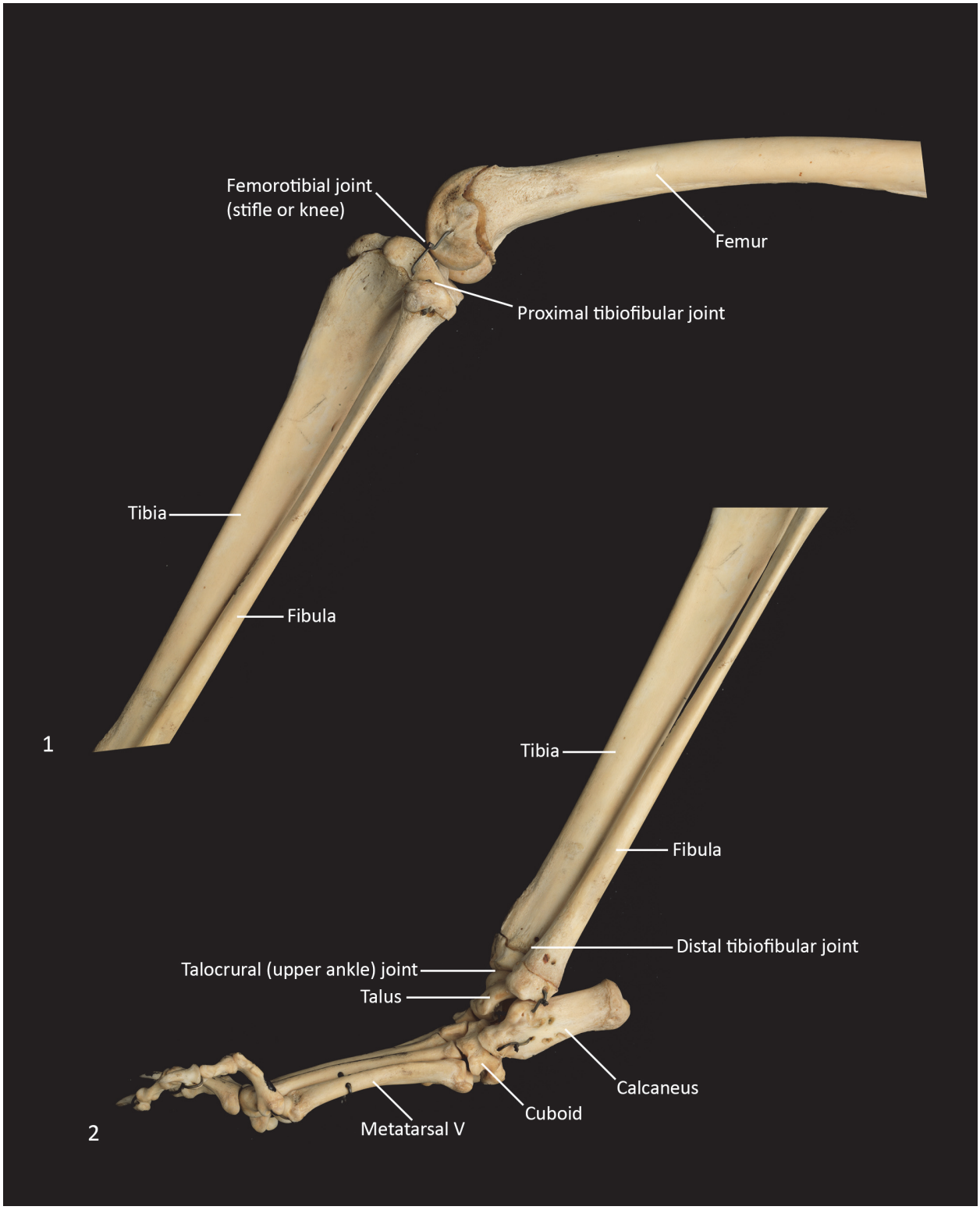

FIGURE 34. 1-2, Stifle (knee) (**1**) and ankle regions (**2**) of the left hindlimb of WAM M195 (M3318). Lateral view.

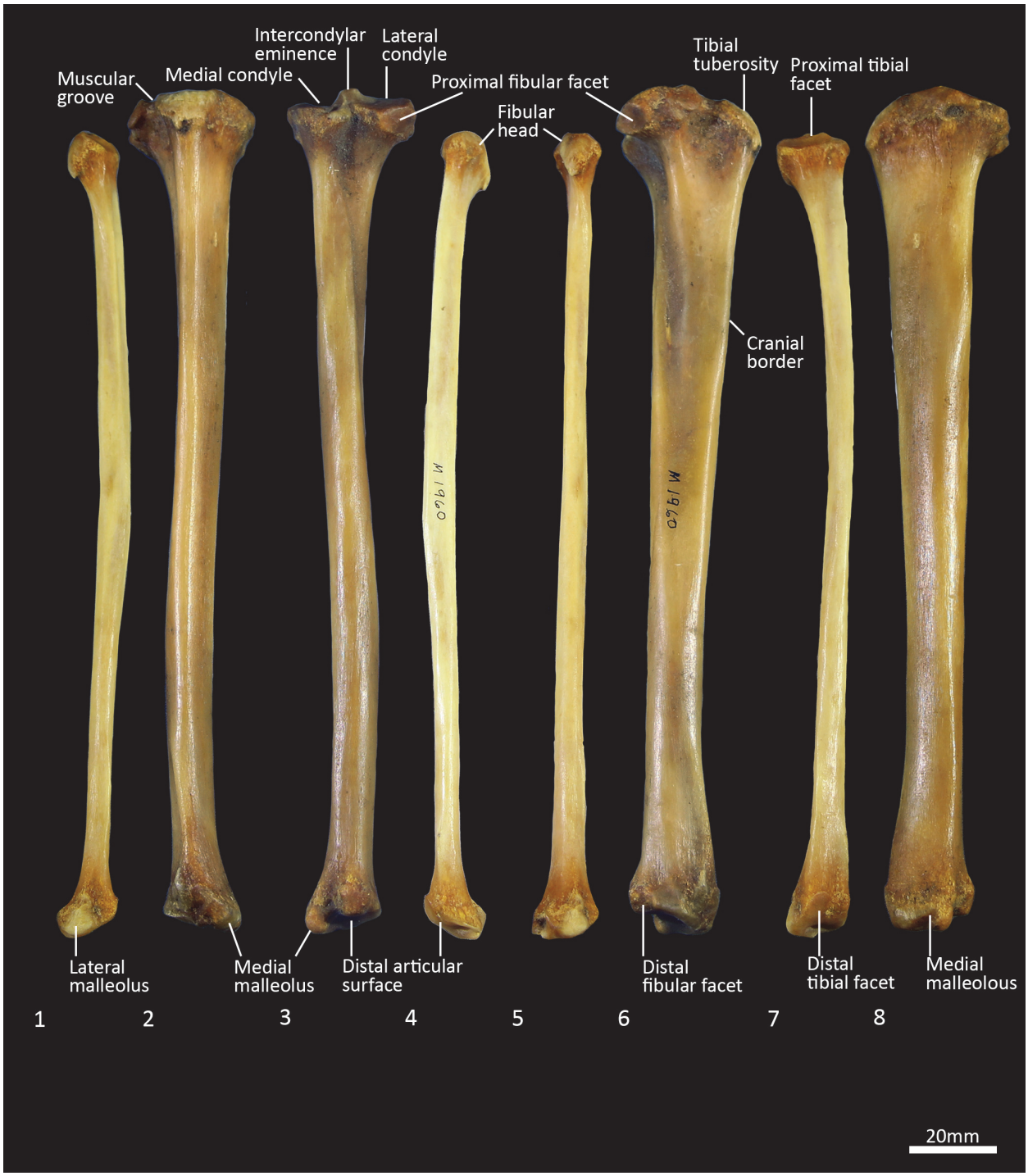

FIGURE 35. Tibia and Fibula (right) SAMA M1960. **1,** fibula cranial view; **2,** tibia cranial view; **3,** tibia caudal view; **4,** fibula caudal view; **5,** fibula lateral view; **6,** tibia lateral view; **7,** fibula medial view; **8,** tibia medial view. Scale bar equals 20 mm.

FIGURE 36. Tibia and fibula (right) WAM M195 (M3318). **1,** fibula cranial view; **2,** tibia cranial view; **3,** tibia caudal view; **4,** fibula caudal view; **5,** tibia lateral view; **6,** fibula medial view; **7,** tibia medial view; **8,** tibia proximal view; **9,** tibia distal view. Scale bar equals 20 mm.

Fibula (Figures 34-36). The fibula is gracile; the diaphysis is ovoid in transverse section. The head is globular, longer in craniocaudal axis than transversely broad, and has an oblique facet for proximal tibiofibular articulation. The distal shaft is enlarged toward the epiphysis, becoming broader and concave preceding the small, semicircular facet for the distal tibial facet. The lateral malleolus is relatively large and protrudes distolaterally. The distal articular facet for the calcaneus is oblique in orientation and joins onto the malleolus to form a continuous surface with the talar and calcaneal facets.

Calcaneus (Figures 34, 37-38). From dorsal view, the tuber calcanei (calcaneal tuberosity) is long, moderately robust and caudally expanded. The tuber is dorso-ventrally deep from the lateral view; being roughly twice as deep as it is transversely wide. The plantar surface is slightly rugose; there is an ovoid flattened scar toward the caudal extremity. The cranial (anterior) plantar tuberosity on the boundary of the cuboid facet is broad and round. The sustentaculum tali is very broad transversely but quite narrow dorsoventrally, accentuating its medially projecting appearance. The articular facets for the talus present as one smoothly continuous surface; the convex posterior portion passes medially from the smoothly contiguous fibular facet to the projecting sustentacular facet, and then extends cranially into the relatively large, shallowly concave surface for the talar head. The sustentacular portion is projecting and dorsocaudally orientated. There is a large, convex, laterally expanded subtriangular fibular facet. A deep, irregular concave area immediately cranial to fibular contact represents attachment of fibular ligaments. Ventral to these depressions is a ridge which arcs cranioventrally to meet the lateroventral margin of the cuboid facet. From the dorsal view, the cuboid facet is orientated at roughly 45degrees to the long axis of the calcaneus. From the distal view, the cuboid articulation is a single, gently concave, subrectangular facet. Ventrally, there is a small, rugose area separating the cuboid facet from the anterior plantar tubercle. The flexor groove on the medial side of the calcaneus is poorly developed.

Talus (astragulus; Figures 34, 37-38). The body of the talus is transversely broader than long (craniocaudal axis). In articulation, the talar head extends only just beyond the cranial border of the calcaneus and has no articulation with the cuboid. It is hemispherical and articulates solely with the navicular. The trochlea surface of the talus is relatively narrow, shallowly concave and arches craniomedially around the large, projecting bulb of the medial trochlear crest. The surface is also highly proximodistally arched and extends around the caudal end of the talus, reflecting the thylacine's ability to switch between a plantigrade and digitigrade stance in the pes. The malleolar fossa is broad, depressed and irregular in shape, with a clearly marked border. The talar neck is very short and transversely broad, and the head is broad and rounded. The large, single concave facet for articulation with the calcaneus covers the full width of the ventral aspect of the talus.

Navicular (central tarsal bone; Figures 37-38). The body of the navicular is dorsoventrally compressed, with a deeply concave facet for the head of the talus proximally, and a slightly convex, drop-shaped facet for the entocuneiform distomedially. Medially, a deep process extends caudally, wrapping around and bracing the medio-ventral aspect of the talus.

Distal tarsal bones (Figures 37, 39). The cuboid (distal tarsal bone IV) is transversely broad and compressed in the proximodistal axis. The proximal articular surface for the calcaneus is undulating, broadly rectangular and oblique in orientation to the craniocaudal axis of the pes. The medial aspect has a well-developed navicular facet. The distal aspect has three articular surfaces: medially, a shelf for articulation with the ectocuneiform (consisting of a distally-facing and medially-facing component); laterally a small articular facet for the fifth metatarsal; and between these, a larger subtriangular facet for the fourth metatarsal. The ectocuneiform is relatively large; with a small rectangular dorsal face, a dorsoventrally deep body and rounded, robust plantar process. The proximal aspect has narrow articular surfaces for the navicular and cuboid; metatarsal II medially, and metatarsal III distally. The mesocuneiform is small and roughly cuboidal, lying between the navicular proximally and second metatarsal distally. The medial face articulates with the entocuneiform, while the plantar surface is covered by the entocuneiform in articulation. The entocuneiform lies on the plantar surface of the tarsus, articulating with the navicular, mesocuneiform and proximal plantar surface of the second metatarsal. It is elongate in proximodistal axis and dorsoventrally compressed. It is unclear whether the first metatarsal is fused with the entocuneiform or completely absent. There is no clear tarsal or metatarsal arch present, indicating that the flexor tendons were poorly-developed.

Metatarsus (Figures 37, 40). There are four elongate metatarsals, the second and fifth are approxi-

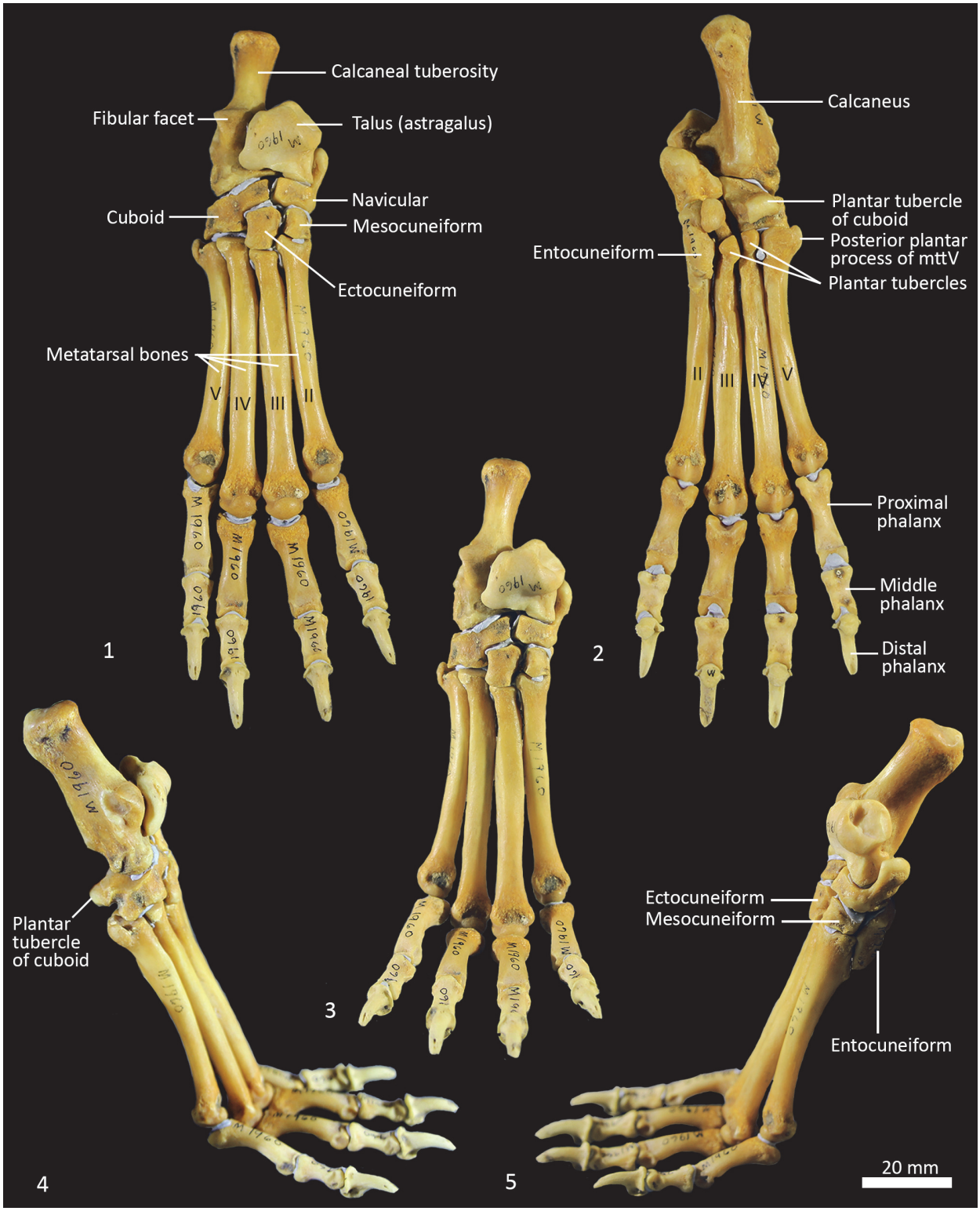

FIGURE 37. Right pes SAMA M1960. **1,** plantar view (plantigrade posture); **2,** dorsal view (plantigrade posture); **3,** cranial view (digitigrade posture); **4,** lateral view (digitigrade posture); **5,** medial view (digitigrade posture). Scale bar equals 20 mm.

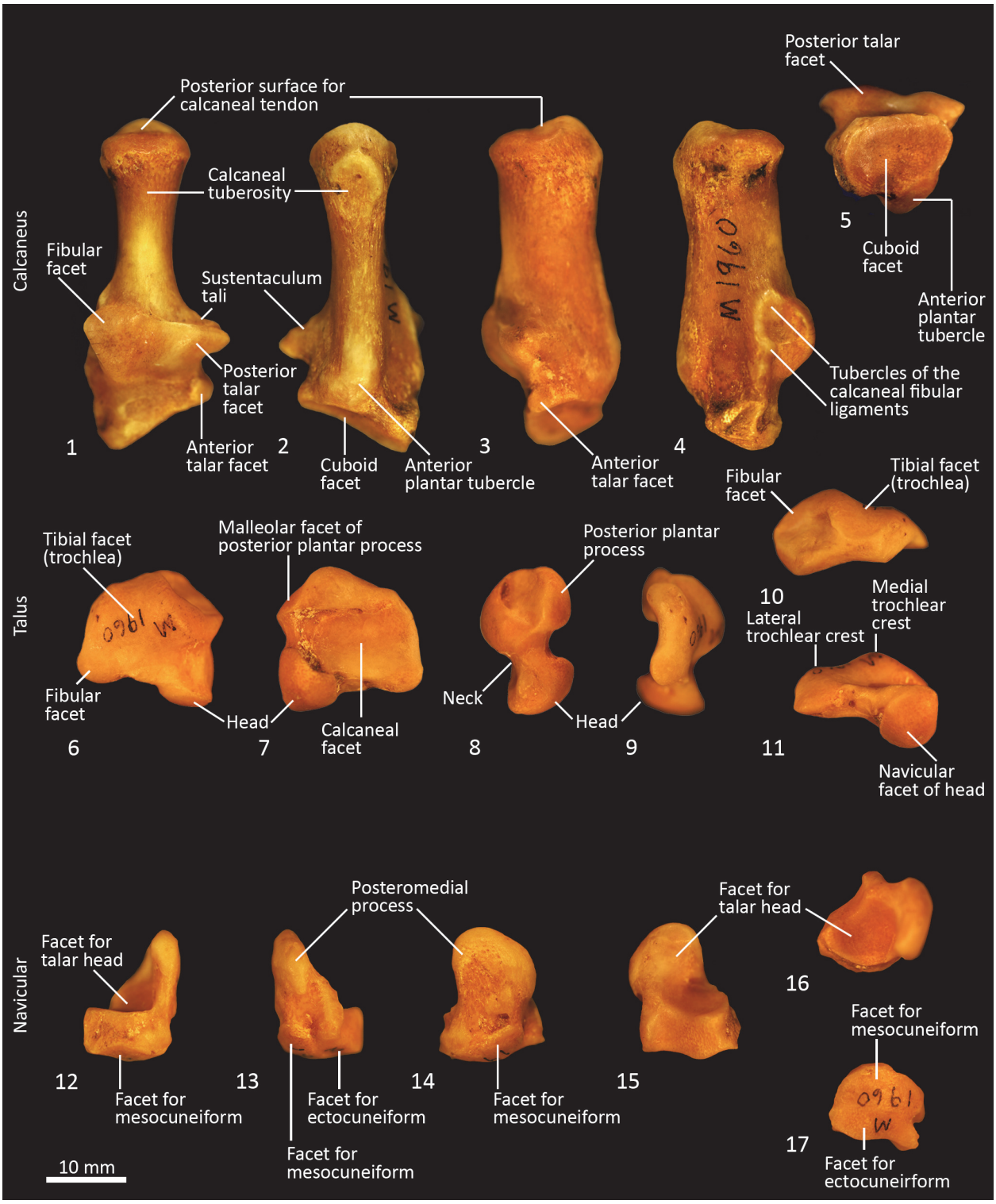

FIGURE 38. Proximal tarsal bones (right pes) SAMA M1960. **1-5,** Calcaneus dorsal (**1**); ventral (**2**); medial (**3**); lateral (**4**); distal views (**5**); **6-10,** talus (astragalus) dorsal (**6**); ventral (**7**); medial (**8**); lateral (**9**); proximal (**10**); **11-17,** distal views; navicular, (central tarsal bone) dorsal (**12**); ventral (**13**); medial (**14**); lateral (**15**); proximal (**16**); distal (**17**) views. Scale bar equals 10 mm.

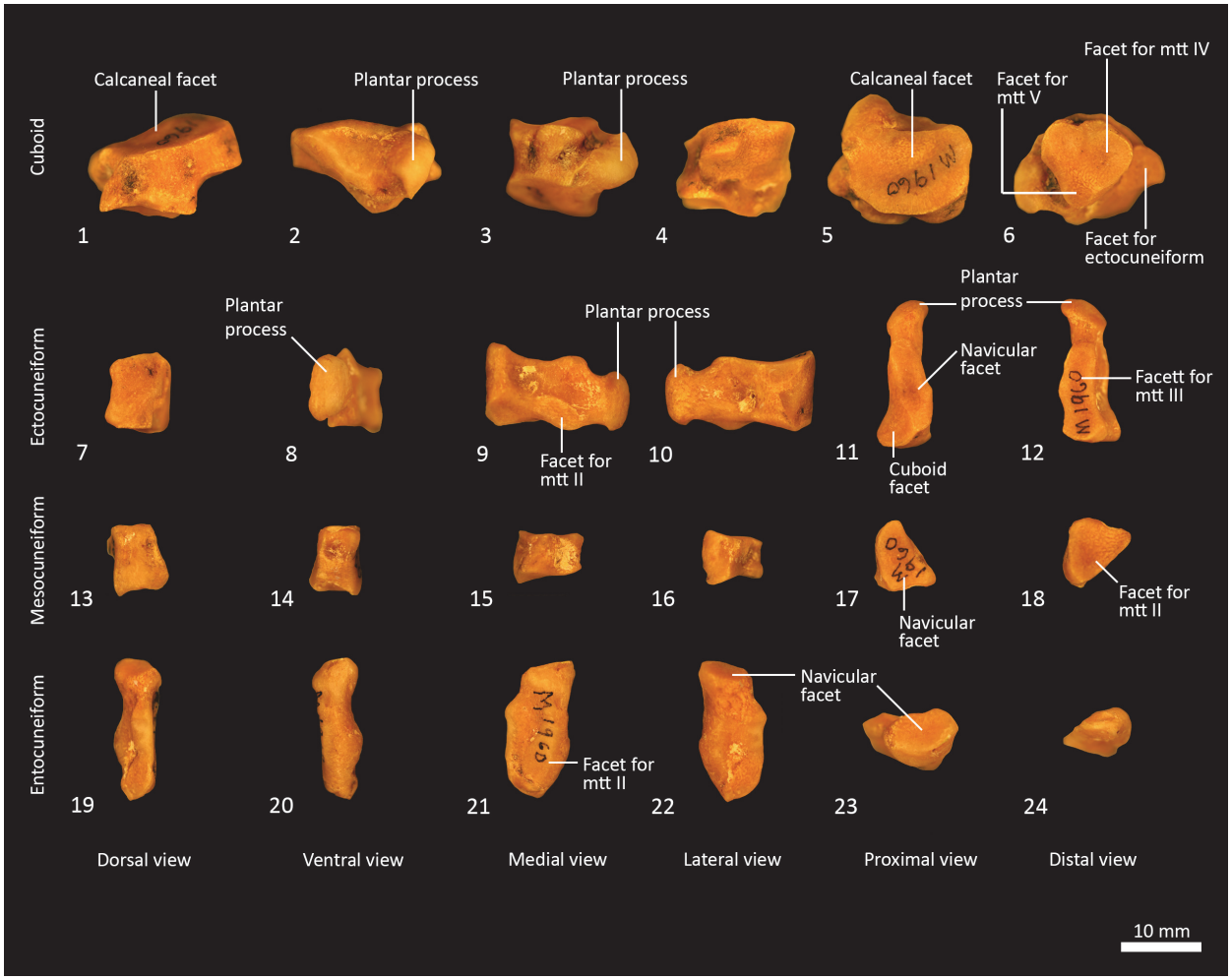

FIGURE 39. Distal tarsal bones (right pes) SAMA M1960. Dorsal, ventral, medial, lateral, proximal and distal views. **1-6,** cuboid; **7-12,** ectocuneiform; **13-18,** mesocuneiform; **19-24,** entocuneiform. Scale bar equals 10 mm.

mately the same length and slightly shorter than the third and fourth. The proximal articular surface of Mt II is subtriangular and roughly as wide as it is deep. The proximal articular surfaces of the third and fourth metatarsals are dorsoventrally deep, with obvious plantar tubercles, and transversely narrow; the fourth with convex margins on either side; the third convex medially and concave laterally. The proximal extremity of the fifth metatarsal has a more rounded articular surface bounded by a small posterolateral process. The diaphysis of each metatarsal is long and gracile; the second flares slightly medially, while the fifth is more distinctly laterally flexed. From the lateral view, the proximal diaphysis is dorsoventrally deep, especially in metatarsals III and IV, and then becomes reduced distally. The distal extremity of each metatarsal is expanded, with large tubercles for the lateral metatarsophalangeal ligaments, and bulbous, rounded articular surfaces with a ventral mesial crest for the metatarsophalangeal joints and flexor sesamoids. The range of movement at the metatarsophalangeal interface is large, reflecting the digitigrade stance employed by thylacines moving at speed.

Phalanges (Figures 37, 40). The proximal phalanges are elongate, approximately one third the length of the corresponding metatarsals, with broad proximal ends, concave ovoid articular surfaces and robust collateral ligament tubercles. The diaphysis is narrowest proximally and expands gently toward the distal extremity. From the lateral view, the proximal phalanges are proximally enlarged, and the shaft is dorsoventrally compressed and dorsally arched. The distal end becomes more robust, supporting a broad, convex articular surface with small circular fossae on either side for the origin of the collateral ligaments. The

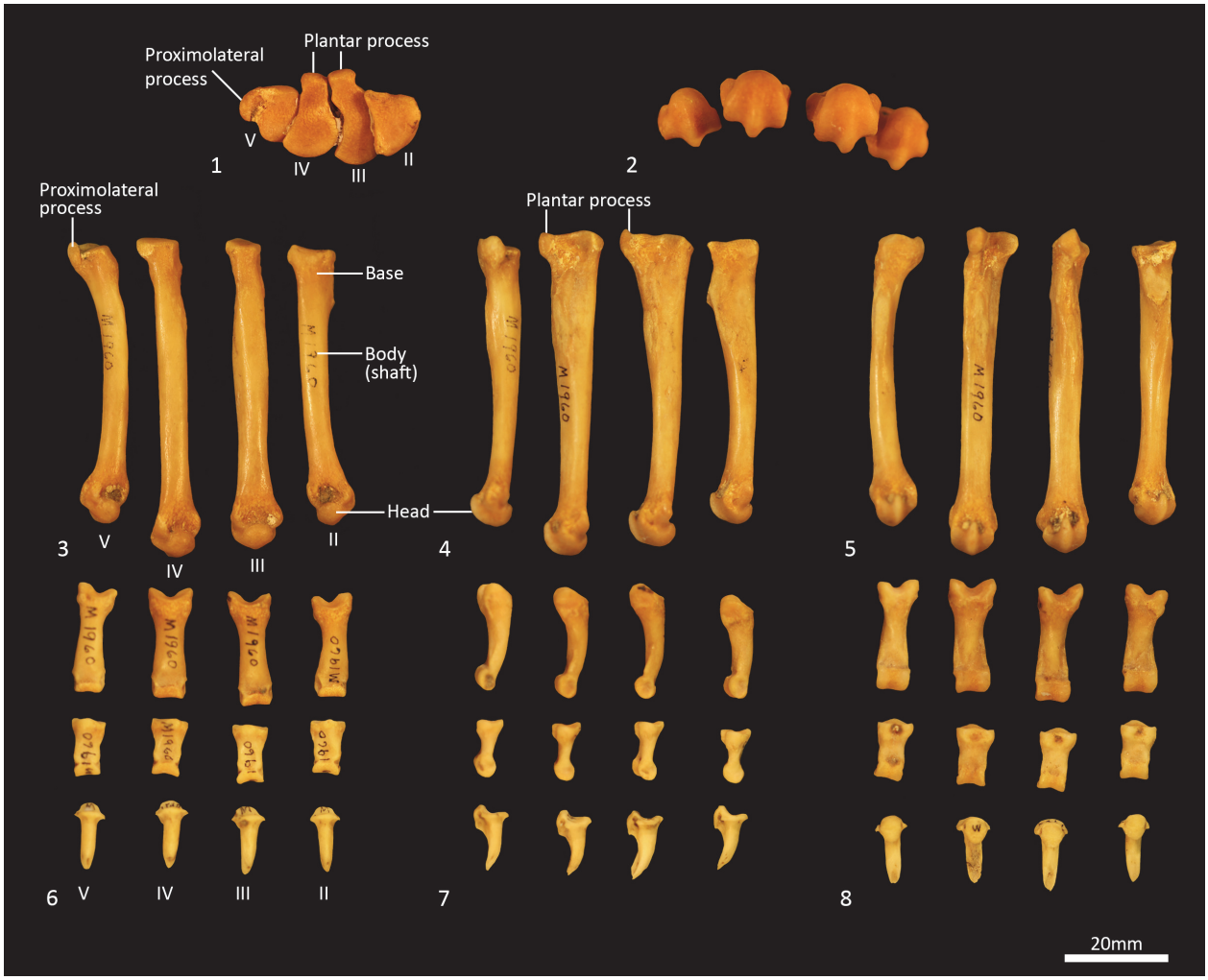

FIGURE 40. Metatarsals and phalanges (right pes) SAMA M1960. **1-5,** metatarsals proximal view (**1**) (not to scale); distal view (**2**) (not to scale); dorsal view (**3**); lateral view (**4**); plantar view (**5**); **6-8,** proximal middle and distal phalanges dorsal (**6**); lateral (**7**); plantar view (**8**). Scale bar equals 20 mm.

middle phalanges are roughly half the length of their corresponding proximal phalanx. They are transversely broader proximally than distally, dorsoventrally compressed, with transversely broad articular surfaces. The distal (ungual) phalanges support strong, moderately curved ungual processes and moderately large, flat flexor tubercles. The flexor tubercles are the same width as the ungual processes, being comparatively less developed than those seen in the manus, and the proximal flaring for bracing the unguis is also less well-developed.

CONCLUSION

Our main objective was to provide a readily accessible and useful illustrated reference of the skeleton of the thylacine for researchers in the fields of zoology, anatomy, and palaeontology. We have not attempted at this point to provide either exhaustive descriptions or comparisons that would be necessary for interpretations of the functional morphology of this unique marsupial. That said, it is tempting to at least make some observations that might then spur on further research into the biology of these animals.

One of the main points of contention with regard to the postcranial skeleton of the thylacine is the extent to which it might be considered adapted for cursorial locomotion, in comparison to placental cursors. Functional interpretations have consistently found that the thylacine was less adapted for cursorial locomotion than eutherian cursors (Jones and Stoddart, 1998; Figueirido and Janis, 2011; Janis and Figueirido, 2014), though this may not be a fair comparison. From the mor-

phology of the bones illustrated herein, it certainly appears to be a very specialized cursor in comparison to other marsupials. The limb bones are relatively 'high-geared', and certainly more so than any other quadrupedal marsupial. For example, the long femur with a small greater trochanter suggests adaptation for a high 'displacement advantage' rather than 'mechanical advantage' and thus investment in limb velocity rather than force output (McHenry, 2012; Young et al., 2014), and the pronounced lesser trochanter suggests importance of the m. iliopsoas for forceful hip flexion. Carpal and tarsal regions of thylacines appear to reflect a more upright, digitigrade stance than that found in other marsupials, in which bony elements are transversely broad and proximo-distally compressed. This would reflect similar changes known for cursorial placental carnivores, where elongate metatarsals and digitigrade stance increase stride length and thus contribute to more efficient locomotion at high speed (Van Valkenburgh, 1987; Carrano, 1997). Thylacines have reduced clavicles, which in placental mammals, is related to a more adducted forelimb posture and greater stride length in cursorial locomotion (Jenkins, 1974). Finally, the greatly reduced epipubic bones may also be related to specialized cursorial locomotion. Marsupials generally have long and well-developed epipubic bones that project forward from the pelvic bones and associated with the abdominal musculature. It has been argued that they play a role in assisting locomotion by supporting some of the muscles that flex the thigh (White, 1989) or stiffen the torso during locomotion (Reilly et al., 2009). As such, epipubic bones would likely reduce flexibility in the lower abdominal region, and we suggest this is linked to the tendency for marsupials to use some kind of bounding gait when moving at speed (though this remains to be tested). The reduced epipubic bones in Thylacines might suggest that they use a more placental-like asymmetrical gait when moving at high speeds. Collectively, these features demonstrate remarkable specialization for cursorial locomotion convergent with eutherian cursors.

ACKNOWLEDGMENTS

We thank D, Stemmer for access to the South Australian Museum collection, C. Corvaia from the WA Museum Conservation department, for her advice on how to relabel the WAM specimen, and two volunteers, P. Norrish and B. Timmerman, for preparing the specimen.

REFERENCES

Archer, M. 1974. New information about the Quaternary distribution of the thylacine (Marsupialia, Thylacinidae) in Australia. *Journal of the Royal Society of Western Australia,* 57:43.

Archer, M. 1976. The dasyurid dentition and its relationships to that of didelphis, thylacinids, borhyaenids (Marsupicarnivora) and peramelids (Peramelina: Marsupialia). *Australian Journal of Zoology, Supplements*, 39:1-34.

Attard, M.R.G., Chamoli, U., Ferrara, T.L., Rogers, T.L., and Wroe, S. 2011. Skull mechanics and implications for feeding behaviour in a large marsupial carnivore guild: the thylacine, Tasmanian devil and spotted-tailed quoll. *Journal of Zoology,* 285(4):292-300. https://doi.org/10.1111/j.1469-7998.2011.00844.x

Beck, R.M.D. 2008. A dated phylogeny of marsupials using a molecular supermatrix and multiple fossil constraints. *Journal of Mammalogy,* 89:175-189. https://doi.org/10.1644/06-mamm-a-437.1

Bednarik, R.G. 2013. Megafauna depictions in Australian rock art. *Rock Art Research,* 30:197.

Bensley, B.A. 1903. III. On the evolution of the Australian Marsupialia; with remarks on the relationships of the marsupials in general. *Transactions of the Linnean Society of London,* 9:83-217. https://doi.org/10.1111/j.1096-3642.1903.tb00447.x

Black, K.H., Archer, M., Hand, S.J., and Godthelp, H. 2012. The rise of Australian marsupials: a synopsis of biostratigraphic, phylogenetic, palaeoecologic and palaeobiogeographic understanding, p. 983-1078. In Talent, J.A. (ed.), *Earth and Life.* Springer, Dordrecht. https://doi.org/10.1007/978-90-481-3428-1_35

Cairns, K.M., Brown, S.K., Sacks, B.N., and Ballard, J.W.O. 2017. Conservation implications for dingoes from the maternal and paternal genome: Multiple populations, dog introgression, and demography. *Ecology and Evolution,* 7:9787-9807. https://doi.org/10.1002/ece3.3487

Carrano, M.T. 1997. Morphological indicators of foot posture in mammals: a statistical and biomechanical analysis. *Zoological Journal of the Linnean Society*, 121:77-104. https://doi.org/10.1006/zjls.1996.0087

Cunningham, D.J. 1878a. The nerves of the fore-limb of the Thylacine (*Thylacinus cynocephalus* or *harrisii)* and Cuscus (*Phalangista maculata*). *Journal of Anatomy and Physiology,* 12(3):427-433.

Cunningham, D.J. 1878b. The intrinsic muscles of the hand of the Thylacine (*Thylacinus cynocephalus*), Cuscus (*Phalangista maculata*), and Phascogale (*Phascogale calura). Journal of Anatomy and Physiology,* 12(3):434-444.

Cunningham, D.J. 1881. The nerves of the hind-limb of the thylacine (*Thylacinus harrisii* or *cynocephalus)* and cuscus (*Phalangista maculata)*. *Journal of Anatomy (London),* 15:265-277.

Cunningham, D.J. 1882. *Report on Some Points in the Anatomy of the Thylacine (Thylacinus cynocephalus), Cuscus (Phalangista maculata), and Phascogale (Phascogale calura), Collected during the Voyage of H.M.S. Challenger in the Years 1873-1876; with an Account of the Comparative Anatomy of the Intrinsic Muscles and Nerves of the Mammalian Pes. Report on the Scientific Results of the Voyage of H.M.S. Challenger during the Years 1873-76, Volume 5, Part 16*. Neill and Co., Edinburgh.

Dawson, L. 1982. Taxonomic status of fossil thylacines (*Thylacinus*, Thylacinidae, Marsupialia) from late Quaternary deposits in eastern Australia, p. 517-525. In Archer, M. (ed.), *Carnivorous Marsupials*, 2. Royal Zoological Society of New South Wales, Mosman.

Dixon, J.M. 1989. Thylacinidae, p. 549-559. In Richardson, B.J. and Walton, D.W. (eds.), *Fauna of Australia*. Australian Government Publishing Service, Canberra.

Figueirido, B. and Janis, C.M. 2011. The predatory behaviour of the thylacine: Tasmanian tiger or marsupial wolf? *Biology Letters,* 7:937-940. https://doi.org/10.1098/rsbl.2011.0364

Flower, W.H. 1876. *An Introduction to the Osteology of the Mammalia: Being the Substance of the Course of Lectures Delivered at the Royal College of Surgeons of England in 18700: With Numerous Illustrations*. Macmillan, London.

Gunn, R.G. 2002. Mudgegonga-2 and the rock art of northeast Victoria. *Rock Art Research,* 19:117-132.

Janis, C.M. and Figueirido, B. 2014. Forelimb anatomy and the discrimination of the predatory behavior of carnivorous mammals: The thylacine as a case study. *Journal of Morphology,* 275:1321-1338. https://doi.org/10.1002/jmor.20303

Jenkins, F.A. Jr. 1974. The movement of the shoulder in claviculate and aclaviculate mammals. *Journal of Morphology,* 144:71-84

Jones, M. 1997. Character displacement in Australian dasyurid carnivores: size relationships and prey size patterns. *Ecology,* 78(8):2569-2587. https://doi.org/10.1890/0012-9658(1997)078[2569:cdiadc]2.0.co;2

Jones, M.E. and Stoddart, D.M. 1998. Reconstruction of the predatory behaviour of the extinct marsupial thylacine (*Thylacinus cynocephalus*). *Journal of Zoology,* 246:239-246. https://doi.org/10.1017/s0952836998010127

Kealy, S. and Beck, R.M.D. 2017. Total evidence phylogeny and evolutionary timescale for Australian faunivorous marsupials (Dasyuromorphia). *BMC Evolutionary Biology,* 17:240. https://doi.org/10.1186/s12862-017-1090-0

Macintosh, N.W. 1964. 4 thousand year old Thylacine tooth (Dasyuridae) + 3 thousand years old dingo skeleton from DJ Mulvaneys archaeological excavations at Fromms Landing Lower Murray River. *Proceedings of the Royal Society of Victoria*, 77:491-425.

McHenry, M.J. 2012. When skeletons are geared for speed: the morphology, biomechanics, and energetics of rapid animal motion. *Integrative and Comparative Biology*, 52:588-596. https://doi.org/10.1093/icb/ics111

Meredith, R.W., Krajewski, C., Westerman, M., and Springer, M.S. 2009. Relationships and divergence times among the orders and families of Marsupialia. *Museum of Northern Arizona Bulletin,* 65:383-406.

Miller, M.E., Evans, H.E., and Christensen, G.C. 1979. *Miller's Anatomy of the Dog,* Second Edition. Saunders, Philadelphia.

Mitchell, K.J., Pratt, R.C., Watson, L.N., Gibb, G.C., Llamas, B., Kasper, M., Edson, J., Hopwood, B., Male, D., and Armstrong, K.N. 2014. Molecular phylogeny, biogeography, and habitat preference evolution of marsupials. *Molecular Biology and Evolution,* 31:2322-2330. https://doi.org/10.1093/molbev/msu176

Murray, P.F. and Megirian, D. 2006. The Pwerte Marnte Marnte Local Fauna: a new vertebrate assemblage of presumed Oligocene age from the Northern Territory of Australia. *Alcheringa Special Issue*, 1:211-228. https://doi.org/10.1080/03115510609506864

Owen, R. 1868. *On the Anatomy of Vertebrates; Mammals*. Longmans, Green and Company, London.

Reilly, S.M., McElroy, E.J., and White, T.D., 2009. Abdominal muscle function in ventilation and locomotion in new world opossums and basal eutherians: Breathing and running with and without epipubic bones. *Journal of Morphology*, 270:1014-1028. https://doi.org/10.1002/jmor.10735

Saltré, F., Rodríguez-Rey, M., Brook, B.W., Johnson, C.N., Turney, C.S.M., Alroy, J., Cooper, A., Beeton, N., Bird, M.I., and Fordham, D.A. 2016. Climate change not to blame for late Quaternary megafauna extinctions in Australia. *Nature Communications,* 7:10511. https://doi.org/10.1038/ncomms10511

Sears, K.E. 2004. Constraints on the morphological evolution of marsupial shoulder girdles. *Evolution,* 58:2353-2370. https://doi.org/10.1111/j.0014-3820.2004.tb01609.x

Sleightholme, S. and Ayliffe, N. 2013. *International Thylacine Specimen Database, 5th Revision*. Zoological Society, London.

Sleightholme, S.R. and Campbell, C.R. 2018. The International Thylacine Specimen Database (6th revision – project summary & final report). *Australian Zoologist,* 39:480-512. https://doi.org/10.7882/az.2017.011

Thomas, O. 1888. *Catalogue of the Marsupialia and Monotremata in the Collection of the British Museum*. British Museum (Natural History), London.

Van Valkenburgh, B. 1987. Skeletal indicators of locomotor behavior in living and extinct carnivores. *Journal of Vertebrate Paleontology*, 7:162-182.

Warburton, N.M. 2006. Functional morphology of marsupial moles (Marsupialia: Notoryctidae). *Verhandlungen des Naturwissenschaftlichen Vereins in Hamburg,* 42:39-149.

Warburton, N.M. and Dawson, R. 2015. Musculoskeletal anatomy and adaptations, p. 53-84. In Klieve, A., Johnston, S., Murray, P., and Hogan, L. (eds.), *Marsupials and Monotremes: Nature's Enigmatic Mammals*. Nova Science Publishers, New York.

Warburton, N.M., Gregoire, L., Jacques, S., and Flandrin, C. 2014. Adaptations for digging in the forelimb muscle anatomy of the southern brown bandicoot (*Isoodon obesulus*) and bilby (*Macrotis lagotis*). *Australian Journal of Zoology,* 61:402-419. https://doi.org/10.1071/zo13086

Westerman, M., Krajewski, C., Kear, B.P., Meehan, L., Meredith, R.W., Emerling, C.A., and Springer, M.S. 2016. Phylogenetic relationships of dasyuromorphian marsupials revisited. *Zoological Journal of the Linnean Society,* 176:686-701. https://doi.org/10.1111/zoj.12323

White, L.C., Saltré, F., Bradshaw, C.J.A., and Austin, J.J. 2018. High-quality fossil dates support a synchronous, Late Holocene extinction of devils and thylacines in mainland Australia. *Biology Letters,* 14(1):20170642. https://doi.org/10.1098/rsbl.2017.0642

White, T.D. 1989. An analysis of epipubic bone function in mammals using scaling theory. *Journal of Theoretical Biology,* 139:343-357. https://doi.org/10.1016/s0022-5193(89)80213-9

Wible, J.R. 2003. On the cranial osteology of the short-tailed opossum *Monodelphis brevicaudata* (Didelphidae, Marsupialia). *Annals of Carnegie Museum,* 72:137-202.

Wroe, S. 1997. A reexamination of proposed morphology-based synapomorphies for the families of Dasyuromorphia (Marsupialia). I. Dasyuridae. *Journal of Mammalian Evolution,* 4:19-52. https://doi.org/10.1023/A:1027379610196

Wroe, S. 2001. *Maximucinus muirheadae*, gen. et sp. nov. (Thylacinidae: Marsupialia), from the Miocene of Riversleigh, north-western Queensland, with estimates of body weights for fossil thylacinids. *Australian Journal of Zoology,* 49:603-614. https://doi.org/10.1071/zo01044

Wroe, S., Clausen, P., McHenry, C., Moreno, K., and Cunningham, E. 2007. Computer simulation of feeding behaviour in the thylacine and dingo as a novel test for convergence and niche overlap. *Proceedings of the Royal Society of London B: Biological Sciences,* 274(1627):2819-2828. https://doi.org/10.1098/rspb.2007.0906

Wroe, S. and Milne, N. 2007. Convergent and remarkably consistent constrain in the evolution of carnivore skull shape. *Evolution,* 61(5):1251-1260. https://doi.org/10.1111/j.1558-5646.2007.00101.x

Wroe, S. and Musser, A.M. 2001. The skull of *Nimbacinus dicksoni* (Thylacinidae: Marsupialia). *Australian Journal of Zoology,* 49:487-514. https://doi.org/10.1071/zo00032

Yates, A.M. 2015. *Thylacinus* (Marsupialia: Thylacinidae) from the Mio-Pliocene boundary and the diversity of late Neogene thylacinids in Australia. *PeerJ,* 3:e931. https://doi.org/10.7717/peerj.931

Young, J.W., Danczak, R., Russo, G.A., and Fellmann, C.D. 2014. Limb bone morphology, bone strength, and cursoriality in lagomorphs. *Journal of Anatomy*, 225:403-418. https://doi.org/10.1111/joa.12220